UNIVERSITY OF CALIFORNIA

Los Angeles

Differential responses of the anaerobic oxidation of methane to nitrate amendment in coastal wetland sediments

A thesis submitted in partial satisfaction

of the requirements for the degree Master of Science

in Geochemistry

by

George Vetushko

2026

ABSTRACT OF THE THESIS

Differential responses of the anaerobic oxidation of methane to nitrate amendment in coastal wetland sediments

by

George Vetushko

Master of Science in Geochemistry

University of California, Los Angeles, 2026

Professor Tina Treude, Chair

Wetlands are the largest natural contributor of methane, a potent greenhouse gas, to the atmosphere. The anaerobic oxidation of methane (AOM) is a major sink to methane in coastal wetland sediments and is typically sulfate-dependent. Anthropogenic activity may feed nitrogen pollution into nearby coastal wetlands yet its effect on AOM is poorly understood.

This study utilized isotope-labeling experiments with in vitro sediment (0–3 cm) slurry incubations to identify how nitrate in nitrogen pollution may affect coastal wetland AOM. Nitrate generally suppressed AOM, but its effect was pathway-specific: while sulfate-dependent AOM was suppressed, nitrate/nitrite and sulfate-independent AOM (e.g. iron and humics substances-dependent AOM) was not. Overall, nitrate/nitrite and sulfate-independent AOM

potentially accounted for over half of AOM across the nitrate-amended incubations. Contrary to prior assumptions that sulfate-dependent AOM dominates in coastal wetland sediments, these findings suggest that nitrate pollution may shift dominant AOM pathways to nitrate/nitrite and sulfate-independent AOM.

The thesis of George Vetushko is approved.

Amy Mainzer

Peng Ni

Xuefeng Peng

Tina Treude, Committee Chair

University of California, Los Angeles

2026

Table of Contents

List of Figures

List of Tables

Acknowledgements

I would like to extend my deepest thanks to my advisor, Prof. Tina Treude, who has mentored me since I first approached her as an undergraduate interested in astrobiology. You have absolutely transformed my understanding of and experience with scientific research, providing opportunities I never could have dreamed of, and I will continue to cherish and carry everything you have taught me into my PhD. I look forward to future collaborations and workshops abroad, and I hope to make you proud in Potsdam.

I would also like to thank my thesis committee members, Prof. Xuefeng Peng, Prof. Peng Ni, and Prof. Amy Mainzer for their valuable insight, tutelage, and guidance for my future. Thank you to the EPSS administrative staff who have supported me throughout my graduate career: Eric Wessenauer, Nanette Capulong, Michael Rathjen, Sean Silverstein, Shannon Yu, Zach Lacson, Omar Abuassaf, Kelli Yang, and Tasha Taylor.

Thank you to the Treude Lab members Jiarui Liu, Emily Klonicki-Ference, Rhegan Thomason, Max Packebush, DJ Yousavich, Sebastian Krause, Sofie Sundberg, Yuzuna Kudo, and Daria Rego. Your advice, friendship, and collaborative support made every day in lab a joy.

Finally, I would like to thank my friends and grandparents for your compassion, love, and support no matter the distance. Dedushka, I'm still looking for life on Mars.

This work was performed in part at the University of California UC Nature Carpinteria Salt Marsh Reserve (DOI:10.21973/N3X08Q) with additional permission from the Sandyland Protective Association. This material is based upon work supported by UC Nature, the California Institute for Biodiversity, the Sea and Sage Audubon Society, and the National Science Foundation Graduate Research Fellowship Program under Grant No. DGE-2034835.

Differential responses of the anaerobic oxidation of methane to nitrate amendment in coastal wetland sediments

George Vetushko[1], Daria Rego[1], Jiarui Liu[1], Qintiantian Nong[2], Annie Bourbonnais[2], Xuefeng Peng[2], Tina Treude[1]

[1]Department of Earth, Planetary, and Space Sciences, University of California Los Angeles, Los Angeles, CA, USA

[2]School of the Earth, Ocean, and Environment, University of South Carolina, Columbia, SC, USA

1. Introduction

1.1 Methane and its global budget

Methane (CH_4) is the second most important greenhouse gas driving climate change with a warming potential ~25 times greater than that of carbon dioxide (Dlugokencky et al., 2011; Legg, 2021; Nisbet et al., 2019). Recent work has estimated global CH_4 emissions at ~575-669 Tg yr^{-1} according to bottom-up and top-down approaches, respectively (Saunois et al., 2025). Most of these emissions are due to anthropogenic activity (e.g. fossil fuels, agriculture, landfills, and biomass burning), while the remaining emissions originate from natural sources (e.g. wetlands, freshwater systems, and land and oceanic sources) (Saunois et al., 2025). Methane has a relatively short atmospheric residence time (~9 years) in comparison to other greenhouse gases (Intergovernmental Panel on Climate Change (IPCC), 2023; Prather et al., 2012). Therefore, regulating methane emissions is an effective option for mitigating climate change as reducing methane emissions may reduce atmospheric methane concentrations (and associated warming) within a multidecadal timescale (Jackson et al., 2020; Ocko et al., 2021; Shindell et al., 2012; United Nations Environment Programme and Climate & Clean Air Coalition, 2021).

1.2 Microbial methane production and oxidation

In anoxic sediments, microbial methanogenesis can convert carbon dioxide, acetate, and methylated compounds into methane (Reeburgh, 2007; Segers, 1998). In marine anoxic sediments, methanogenesis produces ~380 Tg CH_4 yr^{-1}**,** though only ~10 Tg CH_4 yr^{-1} escapes into the atmosphere (Reeburgh, 2007). As methane diffuses upwards through the sediment, microbial methane oxidation can act as a powerful biofilter that mitigates emissions (Hinrichs & Boetius, 2003; Reeburgh, 2007; Valentine, 2002). In oxic systems, such as marine water columns

and oxic sediments, methane-oxidizing bacteria oxidize methane aerobically (Reeburgh, 2007). In anoxic systems, such as freshwater and marine anoxic sediments, ANaerobic MEthanotrophic archaea (ANME) as well as certain bacterial lineages (e.g. NC10 phylum) oxidize methane via the anaerobic oxidation of methane (AOM) (Boetius et al., 2000; Ettwig et al., 2010; Knittel & Boetius, 2009). Together, aerobic methane oxidation and AOM strongly regulate methane emissions from oxic and anoxic environments, respectively.

Aerobic methane-oxidizing bacteria generally use oxygen as the terminal electron acceptor for oxidizing methane (Wallenius et al., 2021). Conversely, different ANME lineages (ANME-1, ANME-2, ANME-3) may utilize various terminal electron acceptors to oxidize methane in the absence of oxygen (Timmers et al., 2017). These electron acceptors (in order of decreasing energetic favorability at standard conditions) include nitrite (NO_2^-), nitrate (NO_3^-), metal oxides such as manganese (Mn) and iron (Fe), humic substances, and sulfate (SO_4^{2-}) (Table 1).

Table 1. Standard Gibbs free energies (ΔG°′) of AOM with different electron acceptors.

Manganese(IV) is in the form of birnessite and iron(III) is in the form of ferrihydrite. Adapted from He et al. (2018) and references therein, and Scheller et al. (2016).

Electron Acceptor	**Reaction**	**ΔG°′ (kJ mol^{-1} CH_4)**
Sulfate	$CH_4 + SO_4^{2-} \rightarrow HCO_3^- + HS^- + H_2O$	-16.6
Humic Substances	$CH_4 + 4AQDS + 3H_2O \rightarrow HCO_3^- + H^+ + 4AH_2QDS$	-41

Electron Acceptor	Reaction	ΔG°′ (kJ mol^{-1} CH_4)
Iron(III)	$CH_4 + 8Fe(OH)_3 + 15H^+ \rightarrow HCO_3^- + 8Fe^{2+} + 21H_2O$	-81.6
Manganese(IV)	$CH_4 + 4MnO_2 + 7H^+ \rightarrow HCO_3^- + 4Mn^{2+} + 5H_2O$	-494.0
Nitrate	$CH_4 + 4NO_3^- \rightarrow CO_2 + 4NO_2^- + 2H_2O$	-519.8
Nitrite	$CH_4 + 8/3NO_2^- + 8/3H^+ \rightarrow CO_2 + 4/3\ N_2 + 10/3H_2O$	-928

Nitrate and nitrite, an intermediate in nitrate reduction, are highly energetically favorable electron acceptors for AOM (Strous & Jetten, 2004). Here, nitrate and nitrite-dependent AOM is grouped as N-AOM. N-AOM removes nitrate from the environment by converting it to inert nitrogen gas (Table 1). ANME-2d archaea (Haroon et al., 2013) and NC10 phylum bacteria (Ettwig et al., 2010) are capable of N-AOM from nitrate and nitrite, respectively. These microbes are typically found in freshwater environments (Ettwig et al., 2010; Haroon et al., 2013) but can also occur in coastal environments at comparable rates (Dai et al., 2025).

While sulfate is the least energetically favorable electron acceptor for AOM at standard conditions (Caldwell et al., 2008), sulfate-dependent AOM (S-AOM) is the dominant AOM pathway in marine sediments (Knittel & Boetius, 2009; Reeburgh, 2007). Sulfate is the dominant electron acceptor in marine sediments (Jørgensen, 1982); furthermore, sulfate availability generally persists across larger sediment depth ranges than other electron acceptors (Froelich et al., 1979). Additionally, sulfate is typically the first available electron acceptor for AOM as microbially produced methane diffuses upwards through sediment (Iversen & Jorgensen, 1985;

Reeburgh, 2007). S-AOM occurs through a consortium of ANME and sulfate-reducing bacteria (Boetius et al., 2000; McGlynn et al., 2015; Wegener et al., 2015).

AOM may also utilize electron acceptors other than nitrate/nitrite and sulfate, including manganese(IV), iron(III), and humic substances (Table 1). Here, this nitrate/nitrite and sulfate-independent AOM is referred to as N/S-independent AOM. The significance of N/S-independent AOM as a methane sink is not yet well understood (Wallenius et al., 2021), though it has been shown to occur in a wide range of environments. Iron and manganese-dependent AOM have been detected in marine (Beal et al., 2009; Riedinger et al., 2014), brackish (Egger et al., 2015), and freshwater sediments (Leu et al., 2020; Sivan et al., 2011) and are generally attributed to ANME-2d (L. Chen et al., 2022; Leu et al., 2020), though ANME-2a (Aromokeye et al., 2020; Slobodkin et al., 2023) and ANME-1 and ANME-2c (Xiao et al., 2023) have also been implicated. Humics-dependent AOM has been detected in marine (Scheller et al., 2016) and brackish sediments (Valenzuela et al., 2017). ANME-2a and 2c (Scheller et al., 2016) as well as ANME-2d (Bai et al., 2019; Xie et al., 2024) have been implicated in humics-dependent AOM.

1.3 Microbial methane oxidation in wetlands

Wetlands are the predominant natural source for atmospheric methane, producing ~161–175 Tg CH_4 yr^{-1} or ~24–30% of global emissions according to bottom-up and top-down estimates, respectively (Saunois et al., 2025). As wetland methane emissions are expected to rise significantly by 2100, identifying and addressing variables controlling wetland methane emissions is becoming increasingly vital (Gedney et al., 2004; Z. Zhang et al., 2017)

Wetlands can be broadly distinguished as coastal or freshwater. In anoxic sediments of both types of wetlands, microbial methanogenesis produces methane (Reeburgh, 2007; Segers,

1998) which may then be consumed via AOM (Boetius et al., 2000; Knittel & Boetius, 2009) and eventually aerobic methane oxidation in oxic sediment layers and in the overlying water column (Reeburgh, 2007). S-AOM is the dominant driver for brackish (Segarra et al., 2013) and marine coastal wetland AOM (Gao et al., 2022; La et al., 2022), while N-AOM is increasingly considered dominant in freshwater wetlands (Hu et al., 2014; Shen et al., 2017; Zhao & Lu, 2023). Other electron acceptors have also been shown to AOM in freshwater sediments: iron and manganese (Leu et al., 2020; Sivan et al., 2011), humic substances (Bai et al., 2019), and sulfate (Schubert et al., 2011; Segarra et al., 2015). Sulfate can remain a contender for freshwater wetland AOM despite its naturally low freshwater concentrations due to rapid turnover by sulfur oxidation (Segarra et al., 2015).

The methane emission rate per area of freshwater wetlands is considerably higher than that of coastal wetlands (7.1 vs. 1.3 g CH_4 m^{-2} yr^{-1}) (Bridgham et al., 2006, 2013). This difference is partially attributed to the tidal influence in coastal wetlands fueling S-AOM by continuously supplying high sulfate concentrations relative to freshwater wetlands (Wallenius et al., 2021). Furthermore, tidally derived sulfate drives organoclastic sulfate reduction which outcompetes methanogenesis for shared metabolic substrates (hydrogen and acetate), suppressing microbial methane emissions (Jørgensen, 2000; Kristjansson et al., 1982; Oremland & Polcin, 1982). Conversely, freshwater wetlands are comparatively sulfate-depleted, so S-AOM is spatially and concentration limited by sulfate availability (Segarra et al., 2015) and organoclastic sulfate reduction consumes less substrate, leaving more available for methanogenesis (Lovley & Klug, 1986; Winfrey & Zeikus, 1977). Consequently, relative to coastal wetlands, freshwater wetlands may both produce more methane and oxidize less of it, resulting in a higher methane emission rate per area (Bridgham et al., 2006, 2013).

1.4 Wetland nitrogen pollution

Coastal and freshwater wetlands may be influenced anthropogenically through various forms of nitrogen pollution, including agricultural runoff and wastewater drainage, which are projected to intensify with time (Galloway et al., 2003, 2008; Howarth et al., 1996; Kintisch, 2013; Smith et al., 1999). Nitrogen pollution mostly consists of inorganic nitrogen compounds, particularly nitrate (Baker, 1992; Howarth et al., 1996) which is an energetically favorable electron acceptor for AOM (Table 1) and organic matter degradation (Froelich et al., 1979). Nitrogen pollution can increase AOM in freshwater wetlands by stimulating N-AOM (Shi et al., 2017, 2022), the increasingly considered dominant AOM pathway (Zhao & Lu, 2023). Freshwater N-AOM can be limited to uppermost sediment as nitrate concentrations, supplied by overlying water, are naturally low and rapidly consumed resulting in shallow nitrate penetration (~2–4 mm) into sediment (Lorenzen et al., 1998). Nitrogen pollution alleviates this nitrate limitation, providing high concentrations of metabolic substrate (Shen et al., 2015; Shi et al., 2022) that persist with depth, expanding the depth range at which N-AOM can occur (Deutzmann et al., 2014). N-AOM can simultaneously remove nitrate, transforming it into inert nitrogen gas, and methane, a potent greenhouse gas (Table 1). Thus, N-AOM has received attention as a bioremediation strategy for mitigating nitrogen pollution and methane emissions from freshwater wetlands (Contreras et al., 2022; Gómez-Gallego, 2022).

Comparatively less is known about the effects of nitrogen pollution on AOM in coastal wetlands (W. Yang et al., 2023). The prominence of N-AOM among coastal wetlands varies: while S-AOM is generally recognized as the dominant contributor to AOM in coastal sediments (Gao et al., 2022; La et al., 2022; Segarra et al., 2013), some studies have shown N-AOM

activity exceeding S-AOM (He et al., 2019; Wang et al., 2019). In coastal sediments, low concentrations of nitrate are supplied from the overlying water column and are rapidly consumed, generally resulting in shallow nitrate penetration into sediment (Canfield et al., 2005). Nitrogen pollution has been shown to stimulate N-AOM in coastal wetland sediments (Wang et al., 2022) by increasing substrate availability. However, nitrogen pollution may also affect S-AOM and N/S-independent AOM. In environments where both nitrate and less energetically favorable electron acceptors — iron(III), manganese (IV), humic substances, and sulfate (Table 1) — are available, N-AOM is more likely to occur (Strous & Jetten, 2004) and may outcompete S-AOM and N/S-independent AOM due to its energetic advantage. Indeed, in vitro studies have reported suppressed S-AOM at high nitrate concentrations in marine deep-sea (5 mM NO_3^-) (Beal et al., 2009) and coastal wetland sediments (3 mM NO_3^-) (Y. Zhang et al., 2020). Thus, though nitrogen pollution may stimulate N-AOM, its potential suppressing effect on S-AOM and N/S-independent AOM obscures its effect on AOM in coastal wetland sediments. It is therefore important to understand how nitrogen pollution in coastal wetlands may affect the balance between different AOM processes, particularly as nitrogen pollution intensifies.

1.5 Aim of this study

Here, we investigate the effects of nitrate in nitrogen pollution on total AOM (N-AOM + S-AOM + N/S-independent AOM) in coastal wetland sediments (0–3 cm) from the Carpinteria Salt Marsh Reserve. We provide insight into the ongoing response of AOM to nitrate pollution and how this may impact nitrate and methane removal in coastal wetland sediments. We propose the following hypotheses:

(H1) Nitrate amendment stimulates N-AOM, simultaneously supporting methane and nitrate removal.

(H2) In nitrate-amended sediments, S-AOM is suppressed but total AOM is not.

(H3) In the absence of classical electron acceptors, humic substances may serve as an electron acceptor for AOM.

2. Methods

2.1 Study area

The Carpinteria Salt Marsh Reserve (CSMR) is a coastal wetland located in Carpinteria, CA, USA (Fig. 1). From the south and southwest, the wetland is tidally influenced, while from the north, anthropogenic drainage feeds nitrate-rich freshwater (> 4000 μM NO_3^-) into the water column (Page et al., 1995). Following previous literature and nitrate concentration measurements reported in this study (see section 3.1.2), four wetland stations (three northern and one southern) were sampled during low tide. Station coordinates and characteristics were recorded using ArcGIS (Table 2). Station NP1 was directly connected to multiple drainage pipes and exhibited intense algal growth (Fig. 1). Drainage pipe water was also actively feeding into the Station NP1 water column at time of sampling. Station NP2 was directly connected to two drainage pipes, while Station NP3 was ~70 m away (straight line distance) from the nearest drainage pipe feeding into Station NP2 (Fig. 1). Station X was the furthest from a drainage pipe (~375 m straight line distance). Water, sediment, and a sediment core were originally collected from Station NP2 on 12 August 2024 to assess site geochemistry, nitrate penetration depth, and potential nitrate and sulfate reduction rates. On 17 June 2025, water, sediment, and a sediment core were collected from Stations NP1, NP2, NP3, and X to assess site geochemistry and potential AOM rates. On 27 August 2025, water, sediment, and a sediment core were collected from Station NP3 for further potential AOM rate incubations.

Figure 1. A map of the Carpinteria Salt Marsh Reserve and its surrounding vicinity. Sampled stations are marked with blue checkpoints: Stations NP1, NP2, and NP3, and X. Photos of drainage pipes at Station NP1 (taken 17 June 2025) and Station NP2 (taken 12 August 2024) are attached.

Table 2. CSMR sampling station names, coordinates, features, sampling dates, and sample types. Features include nitrogen pollution exposure status and salinity conditions.

Sampling Station	Coordinates (Lat, Long)	Features	Sampling Dates	Sample Types
NP1	34° 24' 19.7"N, 119° 32' 34.5"W	Exposed to nitrogen pollution; low-	17 June 2025	Water column, sediment core,

Sampling Station	Coordinates (Lat, Long)	Features	Sampling Dates	Sample Types
		brackish porewater conditions		sediment (for incubation experiments)
NP2	34° 24' 10.7"N, 119° 32' 02.7"W	Exposed to nitrogen pollution; mid-brackish porewater conditions	12 August 2024; 17 June 2025	Water column, sediment core, sediment (for incubation experiments)
NP3	34° 24' 09.6"N, 119° 32' 00.3"W	Exposed to nitrogen pollution; high-brackish porewater conditions	17 June 2025; 27 August 2025	Water column, sediment core, sediment (for incubation experiments)
X	34° 24' 09.2"N, 119° 32' 27.1"W	Not exposed to nitrogen pollution; marine porewater conditions	17 June 2025	Water column, sediment core, sediment (for incubation experiments)

2.2 Water column, sediment, and sediment core sample collection

Water column samples were collected on-site, filtered (polyethersulfone, 0.22 μm), and transferred to 50 mL plastic centrifuge tubes. Water column salinity during low tide was initially determined in situ with a refractometer (Portable Refractometer, Agriculture Solutions) and later confirmed with ion chromatography (Metrohm 761). Water samples were stored at 4°C in the dark and processed for geochemical analyses within 1 day to a week after collection, depending on the sensitivity of the analysis. Leftover water samples were frozen at -20°C.

Sediment was collected into sterile 1L Duran flasks using polycarbonate rings (10 cm inner diameter, 5 cm total height) with cm markings and metal plates. Based on previous experience, sediment was collected from the surface 0–3 cm to target nitrate-exposed regions. Sediment was stored at 20°C in the dark. After 1 to 2 weeks, a sediment subsample was extracted, transferred to an argon-flushed 50 mL plastic centrifuge tube, and centrifuged at 4300×g for 20 min to extract porewater. Porewater was then filtered (polyethersulfone, 0.22 μm) and analyzed by spectrophotometry (Shimadzu-UV 1800) to ensure the sediment was starved of nitrate, here defined as < 0.5 μM NO_3^- which was the detection limit of the method (García-Robledo et al., 2014). Sediment was then processed for incubation experiments (see section 2.4.1).

Sediment cores were collected in polycarbonate push cores (10 cm inner diameter). Cores were inserted ~15-20 cm deep into subtidal sediment with up to 15 cm of overlying water (all stations), and close to drainage pipes (for Stations NP1 and NP2). Cores were then carefully extracted by sliding a metal plate underneath the core bottom; any core headspace was filled with additional overlying water from the adjacent area, and the cores were sealed. Cores were stored at 4°C in the dark and processed for geochemical analyses 1 day after collection.

2.3 Water column, porewater, and solid phase analyses

For analyses of geochemical parameters, sediment cores were sliced under a constant argon flow to mitigate oxidation. The surface 0–3 to 0–5 cm was sliced and processed for all sediment cores in 1 cm increments. Two mL of sediment from each increment was immediately transferred to 10 mL glass serum vials containing 5 mL of 2.5% w/w sodium hydroxide and sealed with grey butyl stoppers and aluminum crimps. Samples were stored upside down in the dark at 4°C until analysis. Methane concentrations were analyzed using a gas chromatograph (Shimadzu GC-2014) with a HayeSep D packed column and flame ionization detector. The column temperature was set to 80 °C, and helium served as the carrier gas at a flow rate of 12 mL min^{-1}. Methane concentrations were calibrated according to standards (Scotty Analyzed Gases) with a precision of ±5%. The remaining sediment from each 1 cm increment was transferred to 50 mL argon-flushed plastic centrifuge tubes and centrifuged at 4300×g for 20 min to extract porewater. Porewater was then filtered (polyethersulfone, 0.22 μm) and refrigerated at 4°C until analysis. Leftover porewater was frozen at -20°C.

Water column and porewater ammonium (NH_4^+) and nitrate/nitrite concentrations were measured spectrophotometrically within 1 day of porewater extraction with a detection limit of 1 and 0.5 μM**,** respectively (García-Robledo et al., 2014; Grasshoff et al., 2009). Sulfate and chloride concentrations were measured with ion chromatography with a detection limit of 30 μM (Dale et al., 2015). Samples were measured within 1 month of porewater extraction. Salinity was calculated from chloride concentrations using Knudson's equation (Knudsen, 1901). Analytical precision of all geochemical measurements was determined using replicate analysis of standards with relative standard deviations (σ) of 2 to 5%.

Solid-phase iron(II) and poorly crystalline iron(III), here referred to as microbially reducible iron(III) (Laufer et al., 2020), were extracted from ~0.1 g sediment using 10 mL anoxic 0.5N hydrochloric acid (HCl), following previous methods (Poulton, 2021) modified from Poulton & Canfield (2005). The iron(II) and iron(III) concentrations were determined spectrophotometrically following the ferrozine assay (Stookey, 1970). Highly crystalline iron(III) minerals were not targeted as they are not energetically favorable for microbial iron reduction in brackish and marine wetland sediment on the timescale (< 72 hours) of sediment slurry incubations in this study (Postma & Jakobsen, 1996).

Sediment porosity samples were weighed and dried at 60°C for five days until the dry weight no longer changed. Sediment porosity was then calculated by dividing the difference of wet and dry sediment weight by the wet sediment volume.

2.4 Sediment slurry incubations for metabolic rate determinations

2.4.1 Incubation setup

Sediment was transferred under a constant argon flow to sterilized, nitrogen-flushed glass serum vials (10 mL and 160 mL) and sealed with non-toxic chlorobutyl stoppers (blue Bellco stoppers, 20 mm) and aluminum crimps (Niemann et al., 2015). Serum vials (10 and 160 mL) were then flushed with nitrogen gas (N_2) for 1 and 5 minutes, respectively, to ensure anoxic conditions. The vials were filled with an anoxic and artificial sterile seawater medium(Laso-Pérez et al., 2018) and made bubble-free, resulting in a 1:1 sediment/medium slurry in the 10 mL vials and a 1:4 sediment/medium slurry in the 160 mL vials. The medium pH, salinity, sulfate, and ammonium concentrations were adjusted according to the characteristics of the original station's porewater (average of 0–3 cm). Sediment slurry vials were incubated with $^{15}N\text{-}NO_3^-$,

$^{35}S\text{-}SO_4^{2-}$, and $^{14}C\text{-}CH_4$ to measure nitrate and sulfate reduction and AOM rates, respectively. Incubation experiments were conducted in the dark at 20 °C, simulating approximate in situ conditions, and were placed on a shaking table at 60 rpm.

2.4.2 Determination of potential nitrate reduction rates

Potential nitrate reduction via denitrification and dissimilatory nitrate reduction to ammonium (DNRA) and anammox rates were determined in in vitro incubations utilizing $^{15}N\text{-}NO_3^-$ (sodium nitrate, ≥ 98 atom % ^{15}N, Sigma-Aldrich) and measuring the production of $^{30}N_2$, $^{15}NH_4^+$, and $^{29}N_2$, respectively. Eighteen sediment slurry incubations in 160 mL glass serum vials from Station NP2 (sampled 12 August 2024) were injected to target 187 µM $^{15}N\text{-}NO_3$, simulating on-site water column nitrate concentrations. Half of the incubations were incubated with N_2 only while the other half were incubated with $N_2 + CH_4$ (saturated with methane). At 7, 18, and 24 hours, incubations were terminated in triplicate to form a time series. Killed controls with autoclaved sediment slurry were incubated and terminated in triplicate at each time point.

Incubations were terminated by transferring 12 mL supernatant to N_2-flushed 6 mL vials (two vials per incubation; Exetainer®, Labco, Lampeter, UK) prepared with 0.05 mL of 7 M zinc chloride for preservation until $\delta^{15}N$ analysis using membrane inlet mass spectroscopy (Kana et al., 1994). Two further 10 mL subsamples were filtered (polyethersulfone, 0.22 µm) into 15 mL plastic centrifuge tubes for potential DNRA rate and nitrate and nitrite concentrations measurements. DNRA subsamples were frozen at -20°C for two weeks, thawed and processed to oxidize ammonium to N_2, and measured with membrane inlet mass spectroscopy (G. Yin et al., 2014). Nitrate and nitrite concentrations were stored at 4°C and measured within one day spectrophotometrically (García-Robledo et al., 2014).

Potential nitrate reduction (denitrification and DNRA) and anammox rates were calculated from the slope of the concentrations of $^{30}N_2$, $^{15}NH_4^+$, and $^{29}N_2$, respectively, across the time series by fitting a linear regression divided by the bulk wet sediment volume. The linear regressions utilized the killed controls' average $\delta^{15}N$ for the initial time point, t = 0. Rates were calculated using the following equations, assuming first-order kinetics, derived from Thamdrup and Dalsgaard (2002):

$$(1)\ R_{DF} = \frac{P^{30}}{f_N * V}$$

$$(2)\ R_{DNRA} = \frac{P^{15A}}{f_N * V}$$

$$(3)\ R_A = \frac{P^{29}}{f_N * V}$$

where R_{DF} is the denitrification rate, R_{DNRA} is the DNRA rate, and R_A is the anammox rate; P^{30}, P^{15A}, and P^{29} are the production rates of $^{30}N_2$, $^{15}NH_4^+$, and $^{29}N_2$, respectively, from the linear regressions in mol/day; f_N is the fraction of N that is ^{15}N-labeled; and V is the volume of the bulk wet sediment in cm^3. Production rates of $^{30}N_2$, $^{15}NH_4^+$, and $^{29}N_2$ were then converted to $^{15}NO_3^-$ consumption rates by factoring in the stoichiometric coefficient of denitrification and anammox (2:1 for $^{15}NO_3^-$:$^{30}N_2$ and 1:1 for $^{15}NO_3^-$:$^{29}N_2$, respectively) and DNRA (1:1 for $^{15}NO_3^-$:$^{15}NH_4^+$). As incubations were initially nitrate-starved and all nitrate added was ^{15}N-labeled, f_N was assumed to be 1. DNRA rates may be underestimated as $^{15}NH_4^+$ consumption rates are not accounted for. Rates are expressed as nmol cm^{-3} bulk wet sediment d^{-1}.

2.4.3 Determination of potential sulfate reduction rates

Potential sulfate reduction rates were determined in in vitro incubations utilizing radioactive, carrier-free ^{35}S-SO_4^{2-} (dissolved in Milli-Q water, injection volume 20 µL, activity 204 kBq,

specific activity 37 TBq $mmol^{-1}$) and measuring the production of ^{35}S-labeled total reduced inorganic sulfur (^{35}S-TRIS). Twelve sediment slurry incubations in 10 mL glass serum vials from Station NP2 (sampled 12 August 2024) were divided into four treatments, in triplicate: (i) N_2, low nitrate; (ii) N_2, high nitrate; (iii) $N_2 + CH_4$, low nitrate; and (iv) $N_2 + CH_4$, high nitrate. N_2 incubations were flushed with N_2 only, while $N_2 + CH_4$ incubations were flushed with N_2 and CH_4 (saturated with methane). Low and high nitrate amendments simulated the lowest and highest nitrate concentrations previously measured in the Station NP2 water column, respectively (see section 3.2.2). Incubations lasted 24 hours in total. Incubations were terminated by transferring the slurry to 50 mL plastic centrifuge tubes filled with 20 mL of 20% w/w zinc acetate solution, thoroughly shaking them, and freezing at -30 °C. Killed controls were prepared immediately before incubations were terminated. Sulfate reduction rates were analyzed and calculated according to the cold chromium distillation method (Kallmeyer et al., 2004).

The rate constant (k_{SR}) for sulfate reduction and sulfate reduction rates (R_{SR}) were calculated using the following equations, assuming first-order kinetics:

$$(4)\ k_{SR} = \frac{^{35}\text{S-TRIS}}{^{35}\text{S-TRIS} + ^{35}\text{S-SO}_4^{2-}} * \frac{1}{t}$$

$$(5)\ R_{SR} = k_{SR} * [SO_4^{2-}]$$

where ^{35}S-TRIS is the amount of ^{35}S-labeled total reduced inorganic sulfur produced by sulfate reduction (in counts per minute, cpm); $^{35}S\text{-}SO_4^{2-}$ is the amount of injected ^{35}S-labeled sulfate minus the amount that was reduced to ^{35}S-TRIS (cpm); t is the length of the incubation in days; $[SO_4^{2-}]$ is the concentration of sulfate in the incubation vial in nmol cm^{-3}. Rates are expressed as nmol cm^{-3} bulk wet sediment d^{-1}. Statistical significance in sulfate reduction rates between

incubations with different treatments was assessed using unpaired, two-tailed Student's t-test (equal variances assumed). $P < 0.05$ was considered significant; variability was measured with ± 1σ.

2.4.4 Determination of potential AOM rates

Potential AOM rates were determined in in vitro incubations utilizing ^{14}C-CH_4 by measuring the production of ^{14}C-labeled dissolved inorganic carbon (^{14}C-DIC). Sixteen sediment slurry incubations in 10 mL glass serum vials from Stations NP1, NP2, NP3, and X (sampled 17 June 2025) were saturated with methane and divided into the following treatments in triplicate: (i) nitrate-starved sediment slurry with no additional treatments (N-Starved); (ii) N-Starved slurry with 30 mM molybdate (N-Starved + Mb), a competitive inhibitor for sulfate reduction and associated S-AOM (Liu et al., 2025; Mostovaya et al., 2022); (iii) 0.5 mM NO_3^- amended sediment slurry (N-Amended) to simulate nitrogen pollution (He et al., 2019), within concentrations shown in section 3.1.2; and (iv) 0.5 mM NO_3^- amended sediment slurry + 30 mM molybdate (N-Amended + Mb). Incubations were injected with ^{14}C-CH_4 (dissolved in MilliQ, injection volume 20 µL, ~2.5 kBq, specific activity 185 MBq $mmol^{-1}$, American Radiolabeled Chemicals, USA) and lasted 72 hours. Incubations were then terminated by transferring the slurry to 50 mL glass serum vials with 20 mL 2.5% w/w sodium hydroxide. These vials were quickly closed with rubber stoppers, sealed with aluminum crimps, and thoroughly shaken. Killed controls were prepared immediately before incubations were terminated. AOM rates were analyzed and calculated according to previous methods (Joye et al., 2004; Krause & Treude, 2021).

The effect of nitrate amendment on total AOM (here defined as S-AOM + N-AOM + N/S-independent AOM) was determined by comparing AOM rates in the N-Starved and N-Amended treatments. The effect of nitrate amendment on N-AOM and N/S-independent AOM was determined by comparing the N-Starved + Mb and N-Amended + Mb treatments. The effect of nitrate on S-AOM was then extrapolated. Suggested relative contributions of S-AOM, N-AOM, and N/S-independent AOM to total AOM (%) were determined for the N-Starved and N-Amended treatments using the following equations, multiplied by 100 to convert to %:

N-Starved:

$$(6)\ \text{S-AOM: } 1 - \frac{\text{N-Starved + Mb treatment}}{\text{N-Starved treatment}}$$

$$(7)\ \text{N-AOM} = 0$$

$$(8)\ \text{N/S-independent AOM: } \frac{\text{N-Starved + Mb treatment}}{\text{N-Starved treatment}}$$

N-Amended:

If AOM rates in N-Starved + Mb and N-Amended + Mb treatments were significantly different:

$$(9)\ \text{S-AOM: } 1 - \frac{\text{N-Amended + Mb treatment}}{\text{N-Amended treatment}}$$

$$(10)\ \text{N-AOM: } \frac{\text{N-Amended + Mb treatment} - \text{N-Starved + Mb treatment}}{\text{N-Amended treatment}}$$

$$(11)\ \text{N/S-independent AOM: } \frac{\text{N-Starved + Mb treatment}}{\text{N-Amended treatment}}$$

If AOM rates in N-Starved + Mb and N-Amended + Mb treatments were not significantly different:

$$(12)\ \text{S-AOM: } 1 - \frac{\text{N-Starved + Mb treatment}}{\text{N-Amended treatment}}$$

$$(13)\ \text{N-AOM} = 0$$

$$(14)\ \text{N/S-independent AOM:}\ \frac{\text{N-Starved + Mb treatment}}{\text{N-Amended treatment}}$$

If relative contributions were > 100% or < 0%, they were corrected to 100% and 0%, respectively.

Another 21 sediment slurry incubations in 10 mL glass serum vials from Station NP3 (sampled 27 August 2025) were saturated with methane and divided into the following treatments in triplicate: (i) nitrate-starved sediment slurry with no additional treatments (N-Starved); (ii) 10 mM anthraquinone-2,6-disulfonic acid disodium salt (+ AQDS); (iii) 30 mM molybdate + 4 mM sulfide (+ Mb + S); (iv) 30 mM molybdate + 4 mM sulfide + 10 mM AQDS (+ Mb + S + AQDS); (v) 30 mM molybdate + 4 mM sulfide + 60 mM 2-bromoethanesulfonate (+ Mb + S + BES); (vi) 30 mM molybdate + 4 mM sulfide + 60 mM BES + 100 μM 1,7-octadiyne (+ Mb + S + BES + O); and (vii) 30 mM molybdate + 4 mM sulfide + 60 mM BES + 0.1 g/L penicillin–streptomycin ((+ Mb + S + BES + ANTI) . Incubations were injected with ^{14}C-CH_4 (gaseous, injection volume 10 μL, ~20 kBq, specific activity 185 MBq $mmol^{-1}$, American Radiolabeled Chemicals, USA). Gaseous ^{14}C-CH_4 was used instead of dissolved ^{14}C-CH_4 for greater measurement sensitivity. The incubations were terminated following the same methods previously outlined.

AQDS was utilized as an artificial electron acceptor and analogue for microbially reducible humic substances (Scheller et al., 2016; Valenzuela et al., 2017). Sulfide was utilized to pre-treat sediment (prior to incubation experiments) to consume microbially reducible iron(III) (see section 2.3) and inhibit iron reduction as well as associated iron dependent-AOM (Liu et al., 2025). 4 mM sulfide was the minimum concentration at which dissolved sulfide concentrations

stabilized and were measurable in sediment slurry (~100 μM), indicating that readily reducible oxidants had been exhausted. BES was utilized as a competitive inhibitor of methyl-coenzyme M reductase in ANME and methanogens, inhibiting associated AOM, methanogenesis, and methane-derived dissolved organic carbon (DOC) production (Krause & Treude, 2021; Maltby et al., 2018). 1,7-octadiyne was utilized as a pMMO inhibitor, inhibiting associated aerobic methane oxidation and methane-derived DOC production (Sakoula et al., 2022; Wissink et al., 2024). Penicillin-streptomycin was utilized to stop all bacterial activity, including associated aerobic methane oxidation and methane-derived DOC production (Peng et al., 2021). Humics-AOM rates were determined by comparing the AQDS-treated incubations (+ AQDS and + Mb + S + AQDS) with control treatments (N-Starved and + Mb + S). The treatments including molybdate and sulfide (all treatments with + Mb + S) inhibited sulfate and iron reduction, and associated S-AOM and iron-dependent AOM, potentially diverting some ANME to utilize alternative electron acceptors – here, humic substances, including AQDS.

The rate constant (k_{AOM}) for AOM and AOM rates (R_{AOM}) were calculated using the following equations, assuming first-order kinetics:

$$(15)\ k_{AOM} = \frac{^{14}\text{C-DIC}}{^{14}\text{C-DIC} + ^{14}\text{C-DOC} + ^{14}\text{C-CH}_4} * \frac{1}{t}$$

$$(16)\ R_{AOM} = k_{AOM} * [CH_4]$$

where ^{14}C-DIC is the amount of ^{14}C-labeled DIC produced by AOM (cpm); ^{14}C-DOC is the amount of ^{14}C-labeled DOC produced from methane (cpm); ^{14}C-CH_4 is the amount of residual ^{14}C-labeled methane (cpm); t is the length of the incubation in days; [CH_4] is the concentration of methane in the incubation vial in nmol cm^{-3}. [CH_4] was measured from killed sediment slurry

vials according to the procedure detailed in section 2.3. AOM rates are expressed as nmol cm^{-3} bulk wet sediment d^{-1}.

2.4.5 Determination of potential methane-derived DOC production rates

Potential rates for methane-derived DOC production were measured from Station NP3 sediment slurry (sampled 27 August 2025) by modifying Joye et al. (2004) with the following adjustments. After ^{14}C-DIC was extracted via acidification (Joye et al., 2004), the supernatant from the acidified sediment slurry was subsampled and processed similarly to SW-846 Test Method 9060A: Total Organic Carbon to isolate ^{14}C-DOC (United States Environmental Protection Agency, 2004). First, the supernatant was filtered (polyethersulfone, 0.22 μm) and transferred to 15 mL plastic centrifuge tubes to remove ^{14}C-biomass. The supernatant was then purged for 10 minutes to ensure any remaining ^{14}C-DIC was removed. The purged supernatant was neutralized and centrifuged at 4300×g for 20 minutes to separate supernatant from precipitates. The remaining supernatant was then subsampled, mixed with 10 mL scintillation cocktail (Ultima Gold XR, Perkin Elmer) and measured with liquid scintillation counting. As the sample was previously acidified, volatile organic carbon may have been lost, and reported rates of ^{14}C-DOC production may be underestimated.

Methane-derived DOC production rates were determined by comparing treatments with active methanotrophy (N-Starved, + AQDS, + Mb + S, and + Mb + S + AQDS) with negative control treatments (+ Mb + S + BES, + Mb + S + BES + O, and + Mb + S + BES + ANTI). The + Mb + S + BES treatment served as a negative control where methanotrophy due to ANME was inhibited as well as DOC consumption due to sulfate and iron reduction and methanogenesis. The + Mb + S + BES + O and + Mb + S + BES + ANTI treatments served as negative controls

where all methanotrophic activity (aerobic and anaerobic) was inhibited as well as DOC consumption due to sulfate and iron reduction and methanogenesis.

The rate constant (k_{MDP}) for methane-derived DOC production and methane-derived DOC production rates (R_{MDP}) were calculated using the following equations, assuming first-order kinetics:

$$(17)\ k_{MDP} = \frac{^{14}\text{C-DOC}}{^{14}\text{C-DIC} + ^{14}\text{C-DOC} + ^{14}\text{C-CH}_4} * \frac{1}{t}$$

$$(18)\ R_{MDP} = k_{MT} * [CH_4]$$

Methane-derived DOC production rates are expressed as pmol cm^{-3} bulk wet sediment d^{-1}. Statistical significance in AOM and methane-derived DOC production rates between incubations with different treatments was assessed using unpaired, two-tailed Student's t-test (equal variances assumed). $P < 0.05$ was considered significant; variability was measured with ± 1σ.

2.4.6 Abiotic tracer turnover

To correct for abiotic stable ($^{15}N\text{-}NO_3^-$) and radiotracer ($^{35}S\text{-}SO_4^{2-}$ and $^{14}C\text{-}CH_4$) turnover, reported metabolic rate values are at least the mean tracer turnover in the killed controls plus one standard deviation of the killed control values.

3. Results

3.1 Sediment and water column geochemistry profiles

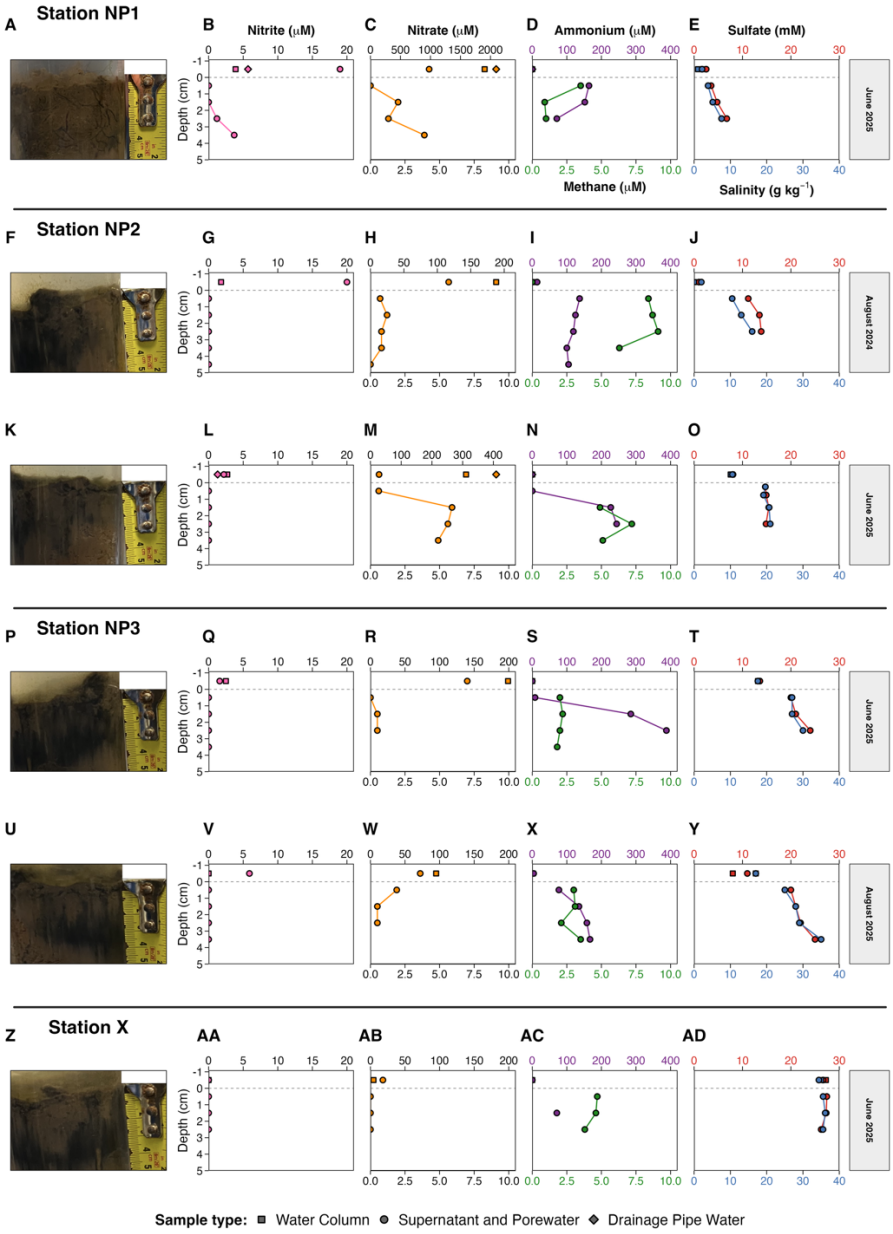

Figure 2. Water column and sediment porewater analyses. Geochemical parameters (nitrite, nitrate, ammonium, methane, sulfate, and salinity) determined in water column samples (negative depth) and sediment porewater (down to 5 cm depth) at the four Carpinteria Salt Marsh

Reserve Stations NP1, NP2, NP3, and X. Each row delineates an individual sediment core. Sampling dates for a given sediment core are recorded on the right side of the figure. Note that sediment cores were collected on multiple dates for Stations NP2 and NP3. A, F, K, P, U, Z: Sediment cores photos (with scale); B, G, L, Q, V, AA: nitrite concentrations; C, H, M, R, W, AB: nitrate concentrations; D, I, N, S, X, AC: ammonium and methane concentrations; E, J, O, T, Y, AD: sulfate concentrations and salinity. Note scale changes on the x-axis and split x-axis scaling for nitrate concentrations (C, H, M, R, W, AB). Note that for Station X average sediment porewater ammonium concentrations (across 0-3 cm) are given due to limited porewater (AC).

3.1.1 Salinity and sulfate concentrations

Sediment porewater (0–4 cm) and water column salinity and sulfate concentrations varied across the stations (Fig. 2E, J, O, T, Y, AD). Note that two concentration ranges are given for Stations NP2 and NP3 as sediment cores were collected on two dates each. The Station NP1 water column was slightly brackish (1 g kg^{-1} salinity, 2 mM SO_4^{2-}) and porewater conditions were low-brackish (4–8 g kg^{-1} salinity, 3–7 mM SO_4^{2-}). The Station NP2 water column ranged from freshwater on 12 August 2024 (0 g kg^{-1} salinity, 0 mM SO_4^{2-}) to mid-brackish on 17 June 2025 (10 g kg^{-1} salinity, 8 mM SO_4^{2-}). Porewater conditions were consistently mid-brackish on both dates: 11–16 g kg^{-1} salinity, 11–14 mM SO_4^{2-} and 19–21 g kg^{-1} salinity, 15 mM SO_4^{2-}. The Station NP3 water column was mid-brackish on both 17 June 2025 (18 g kg^{-1} salinity, 13 mM SO_4^{2-}) and 27 August 2025 (17 g kg^{-1} salinity, 8 mM SO_4^{2-}). Porewater conditions were high-brackish on 17 June 2025 (27–30 g kg^{-1} salinity, 20–24 mM SO_4^{2-}) and 27 August 2025 (25–35 g kg^{-1} salinity, 20–25 mM SO_4^{2-}). The Station X water column (35 g kg^{-1} salinity, 27 mM SO_4^{2-}) and porewater (36 g kg^{-1} salinity, 26–27 mM SO_4^{2-}) were approximately marine.

Stations NP1, NP2, and NP3 had lower salinity in the water column (1, 0–10, and 17–18 g kg^{-1} salinity, respectively) as compared to the porewater (4–8, 11–21, 25–35 g kg^{-1} salinity, respectively) (Fig. 2 E, J, O, T, Y). Additionally, the water column of Stations NP1, NP2, and NP3 had comparatively lower sulfate concentrations (2, 0–8, and 8–13 mM SO_4^{2-}, respectively) than the porewater (3–7, 11–15, and 20–25 mM SO_4^{2-}, respectively). Generally, there was a steady increase in salinity and sulfate concentrations with sediment depth starting at 0–1 cm (4, 11–20, and 25–27 g kg^{-1} salinity; 4, 11–15, and 20 mM SO_4^{2-}) and increasing up to 2–3 cm (8, 16–21, and 29–30 g kg^{-1} salinity; 7, 14–15, and 22–24 mM SO_4^{2-}) for Stations NP1, NP2, and NP3, respectively. At all stations, there were similar trends in salinity and sulfate concentrations in the water column and in porewater across sediment depth.

3.1.2 Inorganic nitrogen concentrations

Water column nitrate and nitrite concentrations were higher at the nitrogen-polluted stations (Stations NP1, NP2, NP3) relative to Station X which was not nitrogen-polluted. Note the difference between nitrate, a dominant component of nitrogen pollution, and nitrite, an intermediate in nitrate reduction, as both are discussed below. At Stations NP1, NP2, and NP3, water column nitrate was high (95–1903 μM NO_3^-) and declined in the sediment core supernatant (28–978 μM NO_3^-) (Fig. 2 C, H, M, R, W), while low nitrite was detected in both the water column (0–3.9 μM NO_2^-) and supernatant (0–20 μM NO_2^-) (Fig. 2 B, G, L, Q, V). In contrast, Station X had low water column nitrate (4.4 μM NO_3^-) that rose slightly in the supernatant (18 μM NO_3^-) (Fig. 2 AB) and no detectable nitrite (Fig. 2 AA).

Sediment porewater nitrate (0–5 cm) was considerably lower (0–5.9 μM NO_3^-) than in the overlying water at Stations NP1, NP2, and NP3 but stayed above detection within 0–3 cm,

indicating nitrate penetration (Fig. 2 C, H, M, R, W). At Station NP1, nitrate and nitrite were not detected within 0–1 cm but were detectable at 1–4 and 2–4 cm, respectively (Fig. 2 B, C). The sediment core exhibited bioturbation in the upper 5 cm (Fig. 2 A) which may have driven nitrate deeper than diffusion could alone. Nitrite was below detection within 0–3 cm at Stations NP2 and NP3.

Water column and sediment core supernatant NH_4^+ concentrations were consistently low (< 3 and < 14 µM, respectively) across all stations, whereas porewater NH_4^+ profiles (0–5 cm) varied between 0–388 µM (Fig. 2D, I, N, S, X, AC). NH_4^+ decreased slightly with sediment depth at Station NP1 on 17 June 2025 and at Station NP2 on 12 August 2024, increased slightly at Station NP2 on 17 June 2025, and increased at Station NP3 on both sampling dates (17 June 2025 and 27 August 2025). At Station X, limited sample volume permitted only determination of the average NH_4^+ concentration in the top 0–3 cm.

Note that water column samples were oxic; thus, concentrations of oxygen-sensitive nitrogen species (ammonium and nitrite) may have been underestimated due to abiotic oxidation.

3.1.3 Methane concentrations

Sediment methane concentrations (0–4 cm) were consistently low (between 0.9 to 9.1 µM) across the stations, with no clear trend (Fig. 2 D, I, N, S, X, AC).

3.1.4 Solid-phase poorly crystalline iron(II) and iron(III) concentrations

Solid-phase poorly crystalline iron(II) and (microbially reducible) iron(III) concentrations were evaluated from Station NP3 sediment (0–4 cm) to assess how much microbially reducible iron(III) was available for iron-dependent AOM in Station NP3 incubations (Fig. 3). On average,

the concentration of microbially reducible iron(III) was ~7 µmol g^{-1}, an order of magnitude less than that of poorly crystalline iron(II) (Fig. 3B).

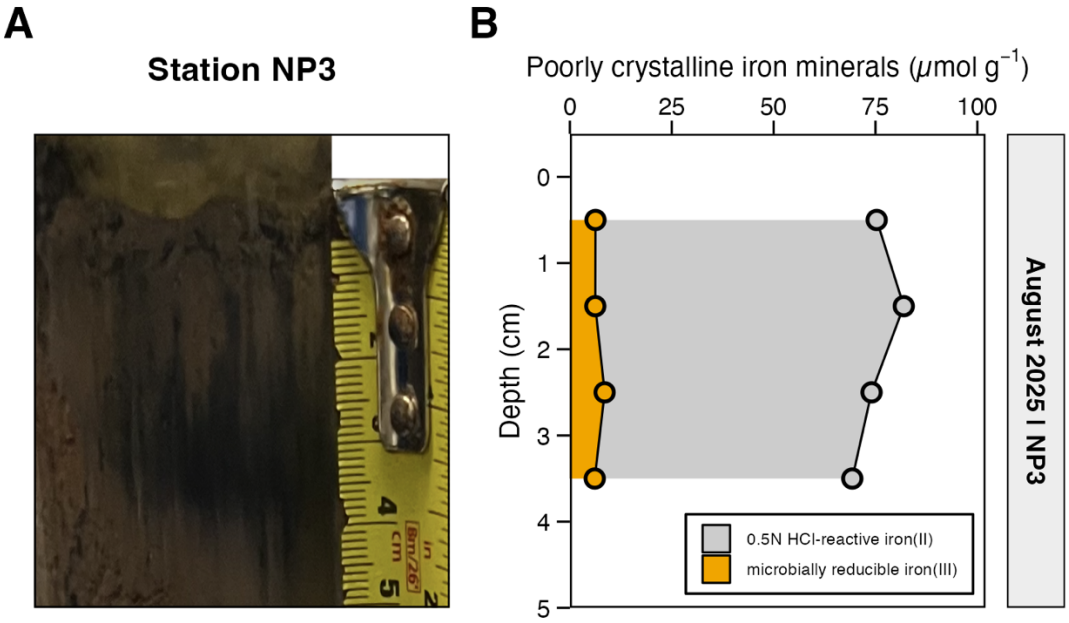

Figure 3. Solid-phase poorly crystalline iron minerals in Station NP3 sediment. Geochemical depth profile determined in a sediment core collected from Station NP3 on 27 August 2025. A: sediment core photo (with scale). B: content of solid-phase poorly crystalline iron(III) and iron(II) minerals.

3.2 Potential microbial metabolic rates

3.2.1 Potential denitrification, DNRA, and anammox rates

Trends in nitrate consumption over time due to potential denitrification, DNRA, and anammox in Station NP2 sediment (0–3 cm) slurry incubations are shown in Figure 4. Potential rates (nmol NO_3^- cm^{-3} bulk wet sediment d^{-1}) under N_2 only and N_2 + CH_4 treatments, respectively, were 301 ± 15 and 330 ± 16 for denitrification, 265 ± 26 and 290 ± 36 for DNRA,

and 7.7 ± 0.7 and 9.1 ± 0.7 for anammox. There was no significant difference in nitrate consumption between N_2 only and N_2 + CH_4 treatments which did not provide evidence for N-AOM ($p > 0.05$). One DNRA incubation (N_2 + CH_4, 24 hours, Replicate 3) was excluded from measurement due to excessive precipitate formation following reaction with hypobromite iodide which posed a risk of equipment clogging.

Across the incubations, nitrate concentrations decreased steadily over time with minor nitrite accumulation consistent with nitrate reduction (Table 3). One killed control sample for nitrate and nitrite concentrations was lost (N2, 17 hours, Killed Control 1), but five other killed controls at the same time point were sampled and are listed. On average, killed controls showed no decrease in nitrate concentration with time, but minor nitrite accumulation was detected. However, there was no detectable denitrification, DNRA, or anammox (no $^{30}N_2$, $^{15}NH_4^+$, and $^{29}N_2$ production, respectively) in the killed controls. This nitrite accumulation may be attributed to low rates of abiotic nitrate reduction associated with sterilization via autoclaving and zinc chloride (Buessecker et al., 2019; Ostrom et al., 2016).

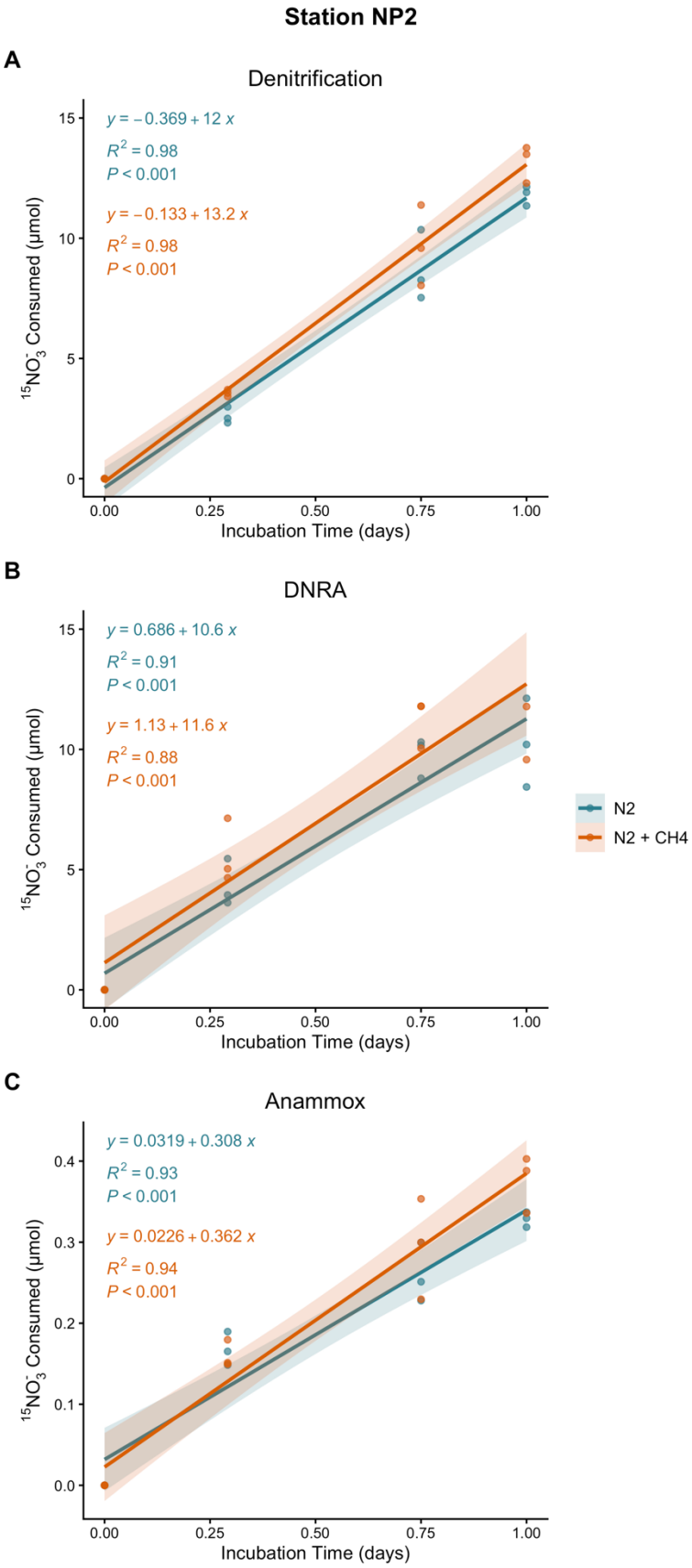
Station NP2
A
Denitrification
y = −0.369 + 12 x
R2 = 0.98
P < 0.001
y = −0.133 + 13.2 x
R2 = 0.98
P < 0.001
15NO3- Consumed (µmol)
Incubation Time (days)
B
DNRA
y = 0.686 + 10.6 x
R2 = 0.91
P < 0.001
y = 1.13 + 11.6 x
R2 = 0.88
P < 0.001
15NO3- Consumed (µmol)
Incubation Time (days)
N2
N2 + CH4
C
Anammox
y = 0.0319 + 0.308 x
R2 = 0.93
P < 0.001
y = 0.0226 + 0.362 x
R2 = 0.94
P < 0.001
15NO3- Consumed (µmol)
Incubation Time (days)

Figure 4. Linear regressions of nitrate consumption over time in Station NP2 sediment slurry incubations. Sediment (0–3 cm) was collected on 12 August 2024. A: $^{15}NO_3^-$ consumption due to $^{30}N_2$ production (denitrification); B: $^{15}NO_3^-$ consumption due to $^{15}NH_4^+$ production (DNRA); C: $^{15}NO_3^-$ consumption due to $^{29}N_2$ production (anammox). Denitrification, DNRA, and anammox rates were calculated by dividing the linear regressions by bulk wet sediment volume (see section 2.3.2). Incubations with N_2 are shown in blue; incubations with N_2 + CH_4 are shown in orange. Linear regressions are plotted with 95% confidence intervals and their respective equations, R^2, and p-values are shown in the top left. Note scale changes on the y-axis.

Table 3. Changes in nitrate and nitrite concentrations (µM) in nitrate reduction rate incubations over time. Incubations were treated with ~187 µM $^{15}N\text{-}NO_3^-$, though actual treatments differed slightly between each incubation (see killed controls below). Prior to treatment, nitrate and nitrite concentrations were below the detection limit (< 0.5 µM).

Incubation ID	Replicate (#)	Time (hours)	Nitrate (µM)	Nitrite (µM)
N_2, Killed Control	1	7	185	0.6
N_2, Killed Control	2	7	209	1
N_2, Killed Control	3	7	207	0.5
N_2 + CH_4, Killed Control	1	7	180	0
N_2 + CH_4, Killed Control	2	7	195	0
N_2 + CH_4, Killed Control	3	7	192	0.6

Incubation ID	Replicate (#)	Time (hours)	Nitrate (µM)	Nitrite (µM)
N_2, Live	1	7	178	1.5
N_2, Live	2	7	119	1.5
N_2, Live	3	7	167	2.4
$N_2 + CH_4$, Live	1	7	177	1.8
$N_2 + CH_4$, Live	2	7	151	1.6
$N_2 + CH_4$, Live	3	7	171	1.7
N_2, Killed Control	1	18	-	-
N_2, Killed Control	2	18	218	3.7
N_2, Killed Control	3	18	174	1.6
$N_2 + CH_4$, Killed Control	1	18	187	0.8
$N_2 + CH_4$, Killed Control	2	18	170	3.9
$N_2 + CH_4$, Killed Control	3	18	171	2.9
N_2, Live	1	18	51	1
N_2, Live	2	18	72	2.3
N_2, Live	3	18	57	2.5
$N_2 + CH_4$, Live	1	18	51	1.9
$N_2 + CH_4$, Live	2	18	72	2.5
$N_2 + CH_4$, Live	3	18	87	2.3
N_2, Killed Control	1	24	204	5.2

Incubation ID	Replicate (#)	Time (hours)	Nitrate (µM)	Nitrite (µM)
N_2, Killed Control	2	24	170	3.8
N_2, Killed Control	3	24	182	4.2
N_2 + CH_4, Killed Control	1	24	178	2.4
N_2 + CH_4, Killed Control	2	24	189	3.4
N_2 + CH_4, Killed Control	3	24	195	2.2
N_2, Live	1	24	0.0	0.5
N_2, Live	2	24	3	1.5
N_2, Live	3	24	0.0	1.2
N_2 + CH_4, Live	1	24	0.0	1
N_2 + CH_4, Live	2	24	10	2.1
N_2 + CH_4, Live	3	24	3	1.4

3.2.2 Potential sulfate reduction rates at contrasting nitrate concentrations

Potential sulfate reduction rates in Station NP2 sediment (0–3 cm) slurry incubations ranged between 178 ± 37.9 and 291 ± 23.2 nmol cm^{-3} bulk wet sediment d^{-1} (Fig. 5A, B). At both low and high nitrate amendments, there was no significant difference in sulfate reduction rates between N_2 only and N_2 + CH_4 incubations ($p = 0.518$ and 0.120, respectively).

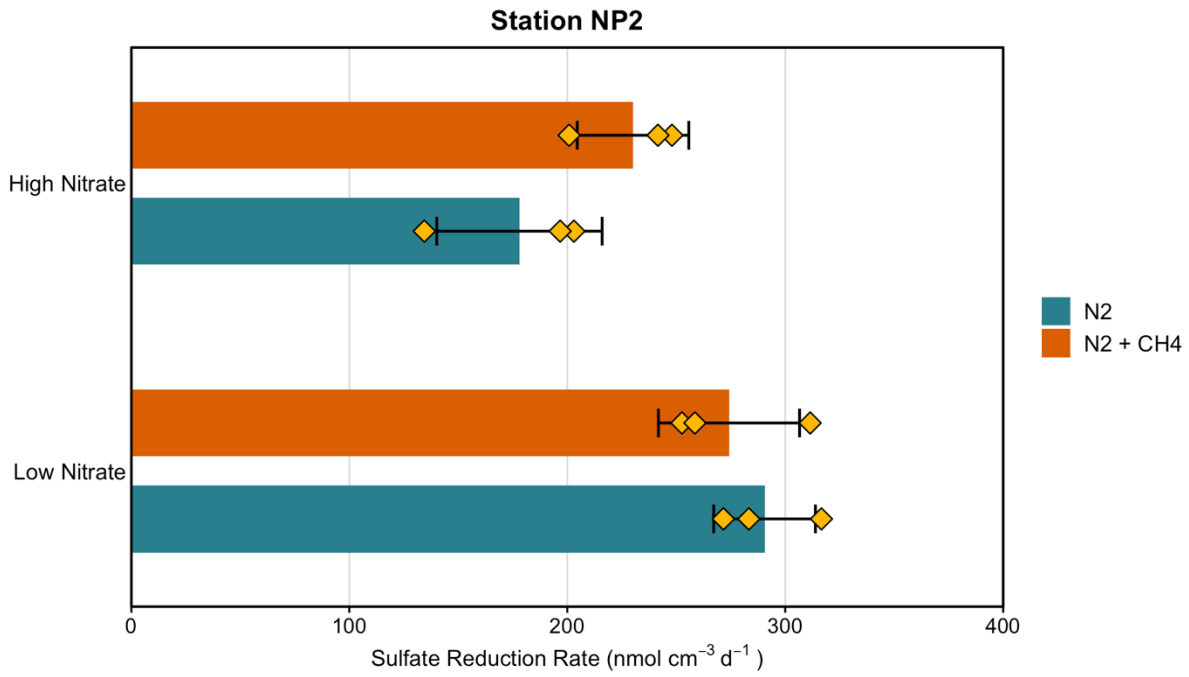

Figure 5. Rates of potential sulfate reduction determined in Station NP2 sediment slurry incubations. Sediment (0–3 cm) was collected on 12 August 2024. Low and high nitrate amendments (8 and 803 µM NO_3^-), simulated lowest and highest measured nitrate pollution, respectively. Incubations with N_2 are shown in blue; incubations with N_2 + CH_4 are shown in orange. Individual replicates are shown as yellow diamonds. Standard deviation is plotted as ± 1σ.

3.2.3 Effect of nitrate amendment on potential AOM rates

Across the stations, potential AOM rates in sediment (0–3 cm) slurry incubations ranged from 0.16 to 4.66 nmol cm^{-3} bulk wet sediment d^{-1} (Fig. 6, A, B, C, D). For Station NP1, the N-Amended treatment had lower AOM rates, on average, relative to the N-Starved treatment. For Stations NP2 and NP3, the N-Amended treatment had significantly lower AOM rates relative to the N-Starved treatment ($p < 0.05$). Station X, which was the furthest from the nearest drainage

pipe (~375 m straight line distance), did not exhibit a significant difference in AOM rates between the N-Amended and N-Starved treatments ($p = 0.57$). The molybdate (+ Mb) treatment for Stations NP1, NP2, and NP3 exhibited significantly lower AOM rates than the N-Starved treatment ($p < 0.05$), suggesting S-AOM was present. Station X exhibited significantly higher AOM rates in the + Mb treatment relative to the N-Starved treatment ($p < 0.05$) which did not provide evidence for S-AOM.

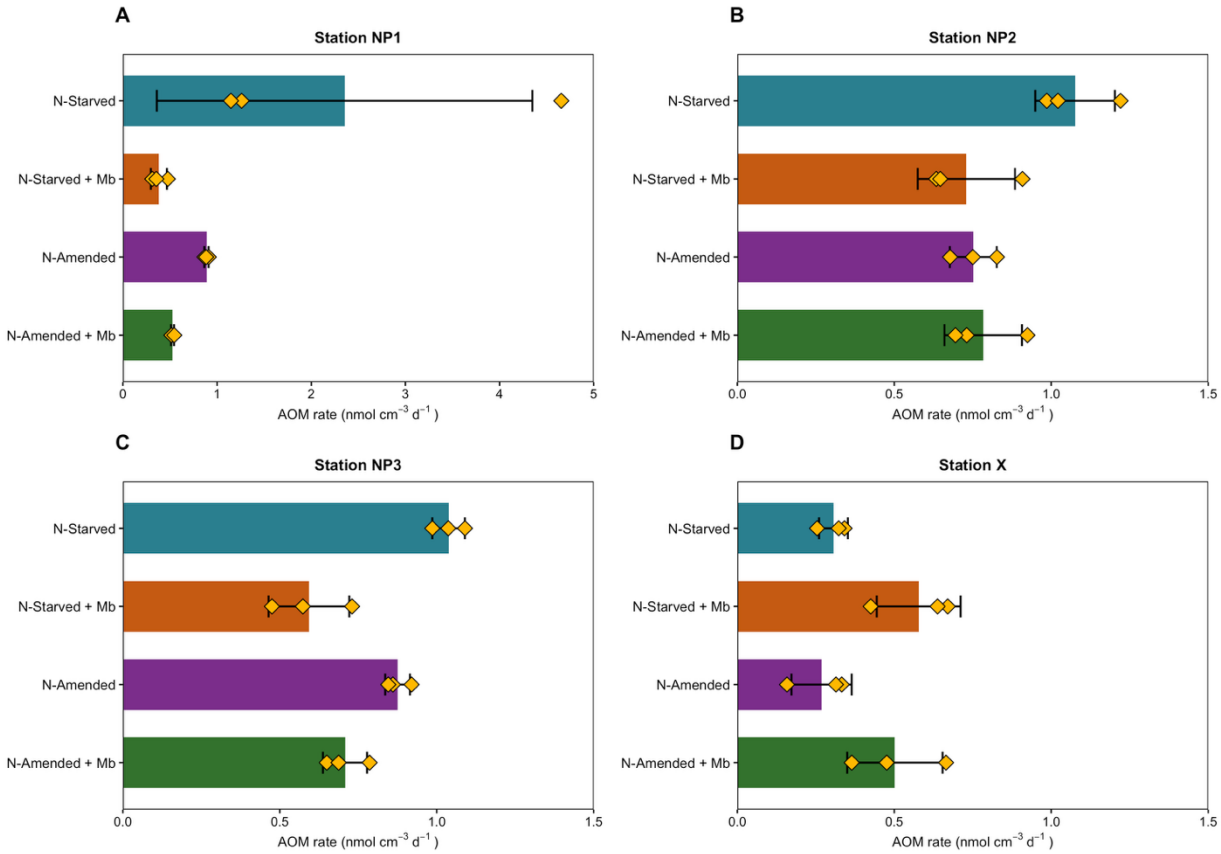

Figure 6. Rates of potential AOM determined in all station sediment slurry incubations. Sediment (0–3 cm) was collected from Stations NP1 (A), NP2 (B), NP3 (C), and X (D) on 17 June 2025. N-Starved refers to nitrate-starved, untreated sediment slurry; N-Starved + Mb refers to N-Starved slurry with molybdate treatment; N-Amended refers to nitrate-amended sediment

slurry; and N-Amended + Mb refers to N-Amended slurry with molybdate treatment. Individual replicates are shown as yellow diamonds. Standard deviation is plotted as ± 1σ.

The relative contributions of S-AOM at Stations NP1, NP2, and NP3 decreased with nitrate amendment (-40%, -32%, and -9%, respectively) while the relative contribution of N/S-independent AOM increased (+27%, +32%, +11%, respectively) (Fig. 7 A, B). In N-Amended incubations, N-AOM contributed to total AOM only at Station NP1 (~16%) (Fig. 7B). N/S-independent AOM contributed ~100% of total AOM at Station X which did not change with nitrate amendment (Fig. 7A, B).

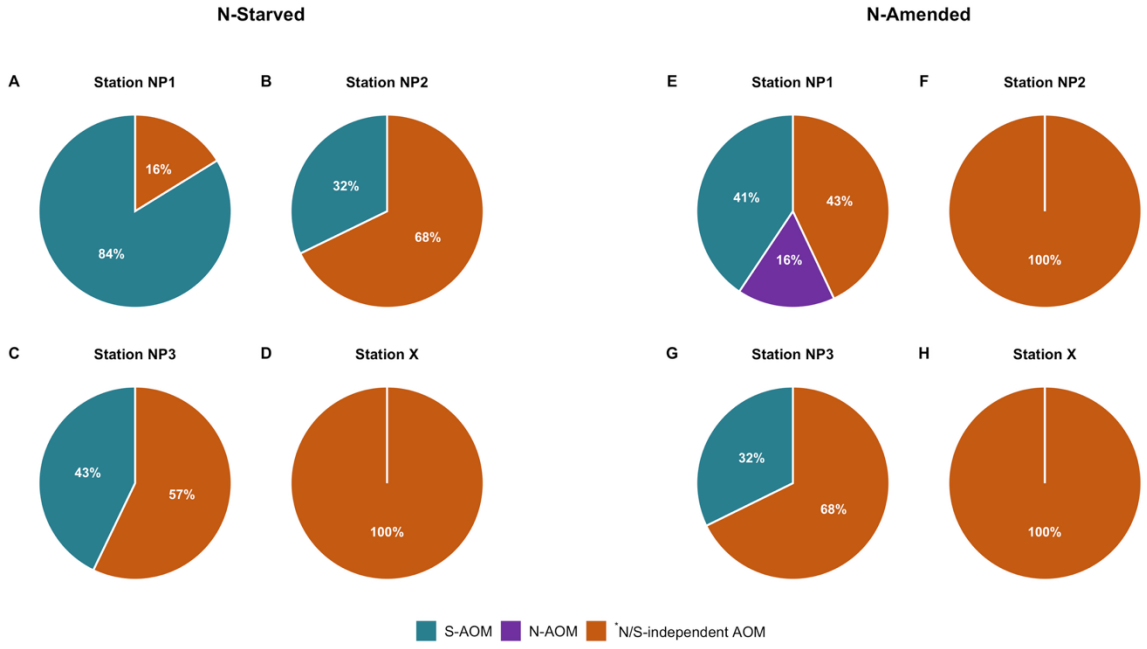

Figure 7. Suggested relative contributions of AOM pathways in all station sediment slurry incubations. Suggested relative contributions of S-AOM, N-AOM, and N/S-independent AOM to total AOM in N-Starved incubations (left panel) and N-Amended incubations (right panel).

Sediment (0–3 cm) was collected from Stations NP1 (A, E), NP2 (B, F), NP3 (C, G), and X (D, H) on 17 June 2025. Corresponding quantitative rates are shown in Figure 6.

3.2.4 Potential humics-dependent AOM and methane-derived DOC production rates

In Station NP3 sediment (0–3 cm) slurry incubations, there was no significant difference in AOM rates between the N-Starved and + AQDS treatments ($p = 0.15$) (Fig. 8A). AOM rates were significantly higher in the + Mb + S + AQDS treatment in comparison to the + Mb + S treatment ($p < 0.05$), indicating that humics-AOM was active when sulfate and iron reduction were inhibited.

Methane-derived DOC production rates ranged from 0–21 pmol cm^{-3} bulk wet sediment d^{-1}. Rates in treatments with active methanotrophy (N-Starved, + AQDS, + Mb + S, and + Mb + S + AQDS) were significantly higher than in negative controls (+ Mb + S + BES, + Mb + S + BES + O, and + Mb + S + BES + ANTI) ($p < 0.05$), indicating methane-derived DOC production (Fig. 8B). Among the treatments with active methanotrophy, rates were significantly higher in the + AQDS, + Mb + S, and + Mb + S + AQDS treatments relative to the N-Starved treatment ($p < 0.05$). Rates significantly decreased with + BES treatment, an AOM and methanogenesis inhibitor, suggesting that methane-derived DOC production may be attributed to ANME or canonical methanogens ($p < 0.05$). Treatments with + O and + ANTI did not significantly change methane-derived DOC production rates relative to + BES treatment which did not provide evidence for methane-derived DOC production linked to aerobic methanotrophy ($p = 0.10$ and $p = 0.15$).

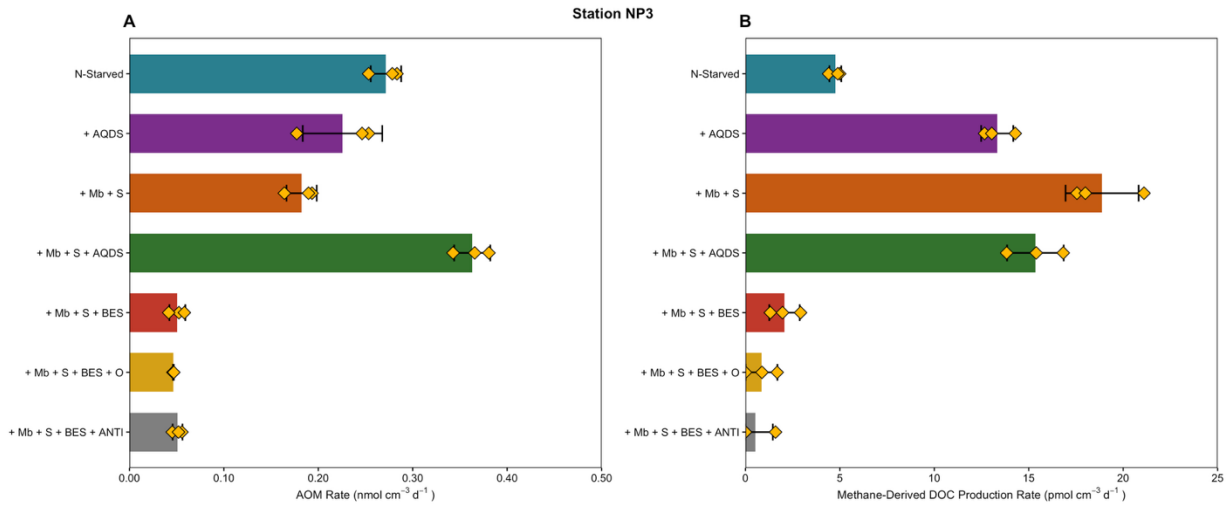

Figure 8. Rates of potential AOM (A) and potential methane-derived DOC production (B) determined in Station NP3 sediment slurry incubations. Sediment (0–3 cm) was collected on 27 August 2025. N-Starved refers to NO_3^- starved, untreated sediment slurry; + AQDS refers to AQDS treatment; + Mb + S refers to treatment with both molybdate and sulfide; + Mb + S + AQDS refers to treatment with molybdate, sulfide, and AQDS; + Mb + S + BES refers to treatment with molybdate, sulfide, and BES; + Mb + S + BES + O refers to treatment with molybdate, sulfide, BES, and 1,7-octadiyne; + Mb + S + BES + ANTI refers to treatment with molybdate, sulfide, BES, and penicillin–streptomycin. Individual replicates are shown as yellow diamonds. Note scale changes on the y-axis. Standard deviation is plotted as ± 1σ.

4. Discussion

This study utilized sediment slurry incubations with stable (^{15}N-NO_3^-) and radiotracer (^{14}C-CH_4 and ^{35}S-SO_4^{2-}) to assess the effects of nitrate in nitrogen pollution on AOM in CSMR sediments (0–3 cm). It is important to note that conditions in slurry incubations were altered relative to in situ environmental settings, which has the potential to shift the dynamics of metabolic processes and microbial communities. However, by implementing substrate and inhibitor treatments, we may elucidate the effects of nitrate amendment on total AOM and constituent AOM pathways (N-AOM, S-AOM, and N/S-independent AOM). We hypothesized that (1) nitrate amendment stimulates N-AOM, simultaneously supporting methane and nitrate removal, (2) in nitrate-amended sediments, S-AOM is suppressed but total AOM is not, and (3) in the absence of classical electron acceptors, humic substances may serve as an electron acceptor for AOM. The following discussion evaluates the hypotheses based on the results of this study and previous research.

4.1 Combined influence of tidal and drainage water input

Tidal and freshwater drainage influenced salinity, sulfate, and nitrate concentrations in the water column and sediment porewater (0–3 cm) at each station. The nitrogen-polluted station (Stations NP1, NP2, and NP3) water columns and porewater were lower in salinity and sulfate concentrations (low to high-brackish) than the marine Station X (see section 3.1.1 and Fig. 2E, J, O, T, Y, AD). Furthermore, the nitrogen-polluted stations had higher water column nitrate concentrations (95–1903 μM NO_3^-) than the marine Station X (4.4 μM NO_3^-) (Fig. 2 C, H, M, R, W, AB). Tidal input likely drove salinity and sulfate concentrations at each station, while

drainage water diluted tidally derived salinity and sulfate and supplied nitrate to the overlying water column and porewater.

At Station X, which was furthest from a drainage pipe (~375 m straight line distance) (Fig. 1), the tidal input signal dominated. Both the Station X water column and porewater retained marine conditions (35–36 g kg^{-1} salinity, 26–27 mM SO_4^{2-}) with low water column nitrate concentrations (4.4 μM NO_3^-) and no nitrate in porewater, suggesting that drainage water input was very low to absent (Fig. 2E, J, O, T, Y, AD). Conversely, at stations directly connected to drainage pipes (Station NP1 and NP2), the drainage water signal was comparatively stronger and diluted tidal input with low to mid-brackish water column (0–10 g kg^{-1} salinity, 0–8 mM SO_4^{2-}) and porewater (4–21 g kg^{-1} salinity, 3–15 mM SO_4^{2-}) conditions and higher water column (188–1903 μM NO_3^-) and porewater (0–5.9 μM NO_3^-) nitrate (Fig. 2 C, H, M, R, W, AB). Station NP3 was more strongly tidally influenced (mid to high brackish conditions) than Stations NP1 and NP2, likely because it was ~70 m straight line distance away from the nearest drainage pipe while Stations NP1 and NP2 which were directly connected to drainage pipes (Fig. 1).

Salinity and sulfate concentrations increased with sediment depth at the nitrogen-polluted stations, suggesting that CSMR sediment, despite drainage water dilution, retains a progressively stronger tidal signal with sediment depth like other coastal wetlands (Gardner, 2007; Moffett et al., 2010). Collectively, each station's water column and porewater salinity, sulfate, and nitrate concentrations likely indicated the frequency and intensity of tidal and drainage water input (Fig. 2).

4.2 N-AOM activity

4.2.1 N-AOM and its contribution to total nitrate reduction and total AOM

The first goal of this study was to evaluate if nitrate pollution stimulated N-AOM and supported nitrate and methane removal via nitrate reduction and AOM, respectively. Similarly to previous studies (Baker, 1992; Howarth et al., 1996), nitrate was the dominant form of nitrogen pollution in the CSMR water column with nitrate concentrations strongly exceeding nitrite and ammonium concentrations (Fig. 2). Nitrate was also the dominant inorganic nitrogen component in drainage pipe water samples taken from Stations NP1 and NP2.

Through radiotracer incubations with ^{14}C-CH_4, N-AOM was detectable at Station NP1 at ~0.15 nmol cm^{-3} d^{-1}; however, only when sulfate reduction was inhibited (Fig. 6). N-AOM was not detectable in any treatments from Stations NP2, NP3, and X. Indeed, previous studies did not detect microbes capable of N-AOM at Stations NP2 and NP3 (Krause et al., 2025). Additionally, detectable N-AOM only in the station with the lowest salinity and sulfate (Station NP1) agrees with previous findings that N-AOM activity negatively correlates with increasing salinity (F. Chen et al., 2021; Frank et al., 2023; Shen et al., 2016) and sulfate (Wang et al., 2019). N-AOM at Station NP2 was also assessed through ^{15}N-NO_3^- incubations and was not detectable (Fig. 4) but demonstrated nitrate reduction rates three orders of magnitude greater than AOM. The lack of N-AOM at Station NP2 could be attributed to organoclastic nitrate reduction fueled by labile organic matter outcompeting N-AOM for nitrate (Legierse et al., 2023). In summary, our combination of ^{14}C-CH_4 and ^{15}N-NO_3^- incubations suggest that nitrate amendment stimulated N-AOM at Station NP1, but not at Stations NP2, NP3, and X.

N-AOM has been shown to remove 0.1–14.6% nitrate (F. Chen et al., 2021) and 2.0–9.5% CH_4 (Hu et al., 2014; W. Yang et al., 2023) in coastal wetlands sediments. We studied total nitrate reduction rates (potentially linked to multiple electron donors, including organoclastic nitrate reduction and N-AOM) only at Station NP2. Assuming total nitrate reduction rates were

at similar orders of magnitude at Stations NP1 and NP2, N-AOM in Sation NP1 would be four orders of magnitude less than total nitrate reduction (Figs. 4, 6). Based on the theoretical ratio of 1 mol CH_4 oxidized with 4 mol NO_3^- (Table 1), N-AOM would contribute ~0.10-0.11% of nitrate removal at Station NP1. This contribution would be at the lower end of the range proposed by Chen et al. (2021).

While nitrate reduction rates were not studied through incubation experiments at Stations NP1, NP3, and X, the presence of nitrate in the station water columns and decline of nitrate within the first few cm of sediment suggests that nitrate was quickly consumed in nature (Fig. 2C, R, W, AB). In the most extreme example, nitrate concentrations at Station NP1 decreased from 1903 μM NO_3^- in the water column to below the detection limit in the first cm of sediment, potentially indicating robust nitrate consumption (Fig. 2C). Furthermore, nitrite, an intermediate in nitrate reduction, was detectable in the water columns and sediment core supernatant and porewater from nitrogen-polluted stations (Fig. 2B, G, L, Q, V). Thus, based on the porewater profiles, nitrate consumption was likely active at all stations, but N-AOM ranged from absent (Stations NP2, NP3, X) to a minor contributor to total nitrate removal (~0.10-0.11% at Station NP1) via nitrate reduction. Because N-AOM was not detected at Stations NP2, NP3, and X, it did not contribute to methane removal (Figs. 6, 7). At Station NP1, N-AOM contributed ~16% of methane removal in nitrate-amended incubations (Fig. 7). This contribution from Station NP1 is higher than ranges proposed by previous studies (2.0–9.5% CH_4) (Hu et al., 2014; W. Yang et al., 2023), while the contributions from Stations NP2, NP3, and X are 0.

The absence of N-AOM activity at Stations NP2 and NP3 could be attributed to the absence of N-AOM capable microbes. A previous study in CSMR did not detect NC10 bacteria or ANME-2d at Stations NP2 and NP3 (Krause et al., 2025), while Station X was not tested.

Additionally, the activity and abundance of N-AOM microbes have been shown to decline with increasing salinity (F. Chen et al., 2021; Frank et al., 2023; Shen et al., 2016) and sulfate concentrations (Wang et al., 2019). Given the mid-brackish to marine conditions at Stations NP2, NP3, and X, salinity and sulfate concentrations could partially account for absent N-AOM. Conversely, the low-brackish conditions at Station NP1 may have been sufficiently low in salinity and sulfate for N-AOM to occur. However, a recent global synthesis (Dai et al., 2025) reported that N-AOM rates in coastal (12.7 ± 2.2 nmol g^{-1} d^{-1}) and freshwater (10.6 ± 1.7 nmol g^{-1} d^{-1}) environments were not significantly different despite the differing salinity conditions. Another explanation is that organoclastic nitrate reducers outcompeted N-AOM microbes (if present) for nitrate (Legierse et al., 2023), suppressing N-AOM. Station NP1 had the highest on-site water column nitrate concentrations (1903 μM NO_3^-) (Fig. 2C) which may have kept nitrate non-limiting and facilitated low N-AOM activity (~0.15 nmol cm^{-3} d^{-1}) alongside organoclastic nitrate reducers. These findings partially support the first hypothesis that nitrate amendment stimulates N-AOM, simultaneously supporting methane and nitrate removal, but only if environmental factors (e.g. presence of N-AOM microbes, salinity, sulfate concentrations, microbial competition, and on-site nitrate concentrations) facilitate N-AOM.

4.2.2 Relative prominence of denitrification, DNRA, and anammox

Stable-isotope incubations with ^{15}N-NO_3^- showed that nitrate reduction rates (301 ± 15 to 330 ± 16 and 265 ± 26 to 290 ± 36 nmol cm^{-3} bulk wet sediment d^{-1} for denitrification and DNRA, respectively) from Station NP2 sediments were similar to or one order of magnitude lower than rates reported for other nitrogen-polluted coastal wetlands (Bourceau et al., 2023; Koop-Jakobsen & Giblin, 2010; Laverman et al., 2006, 2007). Anammox rates (7.7 ± 0.7 to 9.1 ±

0.7 nmol cm^{-3} bulk wet sediment d^{-1}) were similar to those reported for other nitrogen-polluted coastal wetlands (Hou et al., 2015; Koop-Jakobsen & Giblin, 2009) and contributed only a minor fraction of total nitrate consumption relative to denitrification. When compared directly, denitrification and DNRA occurred at similar rates, while anammox rates were roughly two orders of magnitude lower.

Denitrification has been shown to exceed DNRA under high nitrate and low organic carbon conditions (Handler et al., 2022; van den Berg et al., 2016) while DNRA dominates when nitrate is the limiting substrate (Rütting et al., 2011; Tiedje et al., 1983). Here, denitrification and DNRA rates were within the same order of magnitude despite amended nitrate concentrations (187 μM) (Fig. 4). One possible explanation is that sufficiently high DOC concentrations stimulated DNRA. DNRA may be favored over denitrification at $C:NO_3^- > 12$ (Friedl et al., 2018; S. X. Yin et al., 2002). The relative abundance of denitrifying and DNRA microbes may also be relevant (Fazzolari et al., 1990; Tiedje et al., 1983). Alternatively, a recent study demonstrated similar denitrification and DNRA rates in closed-system incubations supplied with both nitrate and sulfate due to metabolic versatility in sulfate-reducing microbes (Bourceau et al., 2023). The study suggested that some sulfate-reducing microbes may switch to DNRA in the presence of nitrate, stimulating DNRA rates (Bourceau et al., 2023). Sulfate-reducing microbes switching to DNRA may have then contributed to the similar order of magnitude in DNRA and denitrification at Station NP2. Desulfobacterales, a canonical sulfate-reducing bacterial class with a key marker gene for DNRA (Bourceau et al., 2023), was previously detected at Stations NP2 and NP3 with a relative abundance of ~10% (Krause et al., 2025). We suggest that microbes within Desulfobacterales were responsible for part of the DNRA rates at Station NP2 incubations treated with $^{15}N\text{-}NO_3^-$, thereby yielding denitrification and DNRA rates of similar magnitude.

4.2.3 Sulfate and nitrate reduction dynamics

Sulfate reduction rates from Station NP2 sediment (178 ± 37.9 to 291 ± 23.2 nmol cm^{-3} bulk wet sediment d^{-1}), determined in radiotracer incubations with $^{35}S\text{-}SO_4^{2-}$, were within the range of other nitrogen-polluted coastal wetlands (Bourceau et al., 2023; Laverman et al., 2012). Interestingly, sulfate and nitrate reduction rates were within the same order of magnitude (~200 and ~600 nmol cm^{-3} bulk wet sediment d^{-1}, respectively) which contrasts with two previous studies of nitrogen-polluted coastal wetlands where nitrate reduction rates exceeded sulfate reduction rates by approximately one order of magnitude (Bourceau et al., 2023; Laverman et al., 2012). However, in these studies the top 0-1 and 0-2 cm of sediment were incubated, while the top 3 cm of sediment was incubated in our study. This difference in depth section selection may be significant as nitrate-reducing microbes often concentrate in the top mm to 1 cm of the sediment, while sulfate-reducing microbes are usually more dominant in deeper sediment (Canfield et al., 2005; Froelich et al., 1979). Thus, the homogenization of the top 3 cm of sediment in this study may have diluted the nitrate-reducing microbial population and enriched the sulfate-reducing one relative to the other studies. Alternatively, nitrate reduction rates in this study may have been concentration-limited: incubation nitrate concentrations (Table 3) were not maintained above the half-saturation constant (~1.5–19.8 μM NO_3^-) for denitrification (Evrard et al., 2013), whereas sulfate reduction was not similarly limited. Nitrate reduction rates may therefore have been artificially decreased relative to sulfate reduction which may partly account for their similar magnitudes. In comparison, nitrate reduction was not concentration-limited in Laverman et al. (2012) but was in Bourceau et al. (2023), and sulfate reduction was not concentration-limited in either previous study.

It is classically assumed that microbial nitrate and sulfate reduction occur at different sediment depths (Canfield et al., 2005; Froelich et al., 1979). This vertical stratification is maintained by nitrate reducers outcompeting sulfate reducers for shared metabolic substrate (e.g. hydrogen and acetate) (Whitmire & Hamilton, 2005). The energetic favorability of nitrate reduction over sulfate reduction gives nitrate reducers a higher affinity for shared substrate, resulting in nitrate reducers maintaining substrate concentrations too low for sulfate reduction to be energetically favorable (Lovley & Goodwin, 1988). However, recent studies have demonstrated simultaneous nitrate and sulfate reduction in freshwater, brackish, and marine sediments (Bourceau et al., 2023; Laverman et al., 2012). Similarly, there was simultaneous nitrate and sulfate reduction in sediment slurry incubations from Station NP2 (Figs. 4, 5). This does not necessarily imply simultaneous activity in situ, as homogenization of the top 3 cm of sediment may have artificially combined vertically stratified nitrate and sulfate-reducing communities. Potentially, drainage-derived nitrate drives nitrate reduction in the top layer of sediment while tidally derived sulfate drives sulfate reduction at successive sediment depths. Nevertheless, these findings challenge the assumption that sulfate reduction may not occur until more energetically favorable electron acceptors, such as nitrate, are fully exhausted (Froelich et al., 1979; Grigoryan et al., 2008; Whitmire & Hamilton, 2005), contributing nuance to the coexistence of nitrate and sulfate reduction.

4.3 Differential effects of nitrate amendment on total AOM, S-AOM, and N/S-independent AOM

4.3.1 Nitrate amendment suppresses total AOM and S-AOM

The second goal of this study was to evaluate if nitrate amendment suppresses S-AOM and total AOM in coastal wetland sediments. This hypothesis that nitrate amendment suppresses S-AOM, but not total AOM, operates under the assumption that N-AOM is active in nitrogen-polluted sediments and compensates for decreases in total AOM due to suppressed S-AOM. However, N-AOM was not detectable at Stations NP2, NP3, and X, and was a relatively minor contributor to total AOM at Station NP1 relative to S-AOM (Fig. 6, 7). As a result, and as further discussed below, N-AOM did not compensate for the suppressing effect of nitrate amendment on S-AOM, resulting in decreased AOM rates.

AOM activity was detected at all stations on the order of ~1 nmol cm^{-3} bulk wet sediment d^{-1} (Fig. 6). However, one N-Starved replicate from Station NP1 exhibited an AOM rate of 4.66 nmol cm^{-3} bulk wet sediment d^{-1}, four times higher than the other replicates, resulting in a high standard deviation relative to the other stations. This higher AOM rate may have been due to a replicate containing sediment micro-niches with higher concentrations of ANME relative to other replicates. Station NP2 and NP3 AOM rates in N-Starved incubations (~1 nmol cm^{-3} bulk wet sediment d^{-1}) were consistent with previously measured AOM rates at these stations under similar incubation conditions (Krause et al., 2025). Krause et al. (2025) also found low abundances of archaea capable of S-AOM and implicated in iron-dependent AOM at Stations NP2 and NP3.

At all nitrogen-polluted stations, nitrate amendment decreased total AOM on average (NP1) and significantly (NP2 and NP3) relative to the N-Starved treatment (Fig. 6). At Station NP1, where nitrate amendment stimulated N-AOM, the suppressive effect of nitrate on total AOM was still more pronounced and resulted in a net decrease in AOM rates. On average, AOM rates decreased by ~62%, ~30%, and ~16% at Stations NP1, NP2, and NP3, respectively. This

decrease may be attributed to nitrate amendment suppressing S-AOM specifically. The relative contribution of S-AOM decreased with nitrate amendment at the nitrogen-polluted stations while the relative contribution of N/S-independent AOM (which may include iron, manganese, and humic substances-dependent AOM) did not (Fig. 6, 7). These findings support the hypothesis that S-AOM is suppressed by nitrate, expanding the concentration threshold for S-AOM suppression from 3–5 mM NO_3^- in previous studies (Beal et al., 2009; Y. Zhang et al., 2020) to 0.5 mM NO_3^- in this study. Furthermore, the previous studies demonstrated S-AOM suppression with artificially low sulfate concentrations (~3 mM) while this study demonstrated it with environmental concentrations (7-28 mM). However, contrary to our hypothesis, total AOM decreased with nitrate amendment. N-AOM was either not active (Stations NP2, NP3) or was not prominent enough (Station NP1) to compensate for suppressed S-AOM (Fig. 6).

Nitrate amendment did not significantly decrease AOM at Station X (Fig. 6), potentially because S-AOM was absent. While S-AOM activity and the suppressing effect of nitrate amendment on S-AOM were detected at the nitrogen-polluted stations (Fig. 6), N/S-independent AOM contributed up to 100% of AOM at Station X (Fig. 7). Where S-AOM is absent, it is plausible that nitrate does not have a suppressing effect on AOM and AOM rates do not significantly decrease. Because N/S-independent AOM accounted for up to 100% of AOM at Station X yet did not decrease, this also suggests that N/S-independent AOM exhibits nitrate tolerance, as further discussed in section 4.3.2.

Nitrate amendment suppressing S-AOM may be due to multiple factors. As nitrate and the intermediate nitrite are more energetically favorable electron acceptors for AOM than sulfate at standard conditions (Table 1), N-AOM may outcompete S-AOM for shared substrate (methane) if nitrate is available (Strous & Jetten, 2004). N-AOM may have competitively suppressed S-

AOM in nitrate-amended incubations from Station NP1 (Figs. 6, 7). However, N-AOM was not detectable at Stations NP2, NP3, and X (Figs. 6, 7) and was therefore unlikely to competitively suppress S-AOM in those stations. Furthermore, it is not clear why nitrate amendment suppressed S-AOM but not N/S-independent AOM as N-AOM is more energetically favorable than both (Fig. 1).

S-AOM occurs through a consortium of ANME and sulfate-reducing bacteria (Boetius et al., 2000; McGlynn et al., 2015; Wegener et al., 2015). Some sulfate-reducing bacteria can switch from sulfate reduction to DNRA when nitrate is available (Bourceau et al., 2023; Krekeler & Cypionka, 1995; Seitz & Cypionka, 1986). At Station NP2, DNRA was detected at rates two orders of magnitude higher than S-AOM (Stations NP1 and NP3 were not tested) (Figs. 4, 6, 7). Given observations from previous studies, it is plausible that some sulfate-reducing bacteria transitioned to DNRA under nitrate-amended conditions, including taxa that may previously have participated in syntrophic associations with ANME during S-AOM. Microbes within Desulfobacterota (reclassified from Deltaproteobacteria), a canonical sulfate-reducing bacterial phylum with a key marker gene for DNRA (Bourceau et al., 2023), have been shown to partner with ANME (including ANME-2c) for S-AOM (Knittel et al., 2005). Desulfobacterota and ANME-2c were previously detected at Stations NP2 and NP3 (Krause et al., 2025). Furthermore, members of Desulfobacterales (a bacterial order within phylum Desulfobacterota and class Desulfobacterales) can participate in S-AOM (Murali et al., 2023) and DNRA (Bourceau et al., 2023), and were detected at Station NP2 and NP3 (Krause et al., 2025). In the presence of nitrate, members of Desulfobacterota/Desulfobacterales may therefore have switched from S-AOM to DNRA (decoupled from AOM), thereby reducing S-AOM rates. This applies to Station NP2 and NP3, where Desulfobacterota/Desulfobacterales has been previously detected. Bacterial diversity

was not evaluated at Station NP1, but Desulfobacterota/Desulfobacterales may have been present there as well.

Nitrate-derived inorganic nitrogen products (nitrite and ammonium) may also have been involved in suppressing S-AOM. Nitrite may competitively inhibit the dissimilatory sulfite reductase enzyme (Wolfe et al., 1994). Additionally, high ammonium concentrations (3 mM) may have a suppressing effect on S-AOM (Y. Zhang et al., 2020). Thus, considerable nitrite or ammonium accumulation in incubations could have contributed to S-AOM suppression. Nitrite and ammonium concentrations were not determined throughout the AOM rate incubations, however, and cannot be evaluated.

4.3.2 Relative tolerance of N/S-independent AOM to nitrate amendment

The effect of nitrate amendment on N/S-independent AOM was determined by comparing the + Mb and + Mb + N treatments (see section 3.2.3). While the relative contributions of S-AOM to total AOM generally decreased with nitrate amendment across the stations, the relative contributions of N/S-independent AOM increased (Fig. 7). As previously mentioned, N/S-independent AOM rates did not increase; rather, N/S-independent AOM contributions increased because S-AOM rates decreased while N/S-independent AOM rates did not change (Figs. 6, 7). As nitrate amendment did not significantly decrease N/S-independent AOM rates in nitrate-amended incubations, this study may suggest that N/S-independent AOM is nitrate tolerant (Fig. 6).

It is not possible to discern exactly which N/S-independent AOM pathways were active in this study. AOM coupled to iron(III) and humic substances are candidates for N/S-independent AOM and can occur in coastal wetlands (Segarra et al., 2013; Valenzuela et al.,

2017, 2019). Additionally, an ANME lineage implicated in iron-dependent AOM was previously detected at Stations NP2 and NP3 (Krause et al., 2025). Differentiating between N/S-independent AOM pathways may be difficult as conventional inhibitors for AOM pathways (e.g. BES) are relatively unspecific and incomplete (Krause & Treude, 2021; Maltby et al., 2018; Timmers et al., 2015). Thus, which N/S-independent AOM pathways were active, and their respective magnitudes, may have varied between incubations. Additionally, it is possible that nitrate amendment suppressed certain N/S-independent AOM pathways in incubations treated with molybdate and nitrate. Assuming N-AOM was active in all stations, the combination of suppressed N/S-independent AOM and stimulated N-AOM may have produced AOM rates significantly higher than (Station NP1) or not significantly different from (Stations NP2, NP3, and X) incubations treated with molybdate only. This combination would falsely indicate that nitrate does not suppress N/S-independent AOM and could have applied to any of the four tested stations. However, as previously discussed (see section 4.2.1), N-AOM was not detected at Stations NP2, NP3, and X, and N-AOM microbes were not previously detected at Stations NP2 and NP3 (Krause et al., 2025). We propose that nitrate tolerance in N/S-independent AOM pathways is a more likely explanation than nitrate simultaneously stimulating N-AOM and suppressing N/S-independent AOM.

4.4 Dominant AOM pathways across a sulfate-salinity gradient

4.4.1 Variable contributions of S-AOM to total AOM among stations

Sulfate reduction is widely considered the dominant pathway driving AOM in marine and brackish sediments, including coastal wetlands (Gao et al., 2022; La et al., 2022; Segarra et al., 2013; Zhao & Lu, 2023). In these sediments, both S-AOM and total AOM increase with sulfate

concentrations and salinity (La et al., 2022; Lee et al., 2025) which are supplied by tidal input (Petersen et al., 2023). It is then expected that S-AOM and its relative contribution to total AOM increase along a sulfate-salinity gradient (La et al., 2022; Lee et al., 2025; Zhao & Lu, 2023) with high-brackish and marine wetland sediments supporting a higher S-AOM contribution than low-brackish and freshwater sediments (Segarra et al., 2013; Wallenius et al., 2021; Xue et al., 2024; Zhao & Lu, 2023).

Under N-Starved conditions, the relative contribution of S-AOM to total AOM did not increase with salinity and sulfate; rather, it decreased on average. Across the gradient of increasing salinity and sulfate, S-AOM contributed ~81%, ~32%, ~43%, and 0% of AOM at Stations NP1, NP2, NP3, and X, respectively (Fig. 7). S-AOM dominated AOM only at Station NP1, the lowest-sulfate, lowest-salinity station. At every other station, the N/S-independent AOM contribution was dominant (57–100%) up to ~100% at the marine Station X. S-AOM was therefore a dominant contributor only in low-brackish sediment incubations under N-Starved conditions, and not in mid/high-brackish or marine sediment, the opposite of the expected trend.

Under N-Amended conditions, S-AOM was not the dominant contributor at any station (<50% of AOM) and the N/S-independent AOM contribution increased at all stations (Fig. 7). Across both treatments, then, the lowest-sulfate station (Station NP1) exhibited the highest S-AOM contribution while the highest-sulfate station (Station X) exhibited the lowest S-AOM contribution. These findings are contrary to the longstanding notion of higher S-AOM activity with increasing salinity and sulfate concentrations (La et al., 2022; Lee et al., 2025; Segarra et al., 2013; Wallenius et al., 2021; Xue et al., 2024; Zhao & Lu, 2023). One precedent for high S-AOM contribution at low sulfate concentrations is its dominance in some freshwater wetlands where sulfate is resupplied through sulfur oxidation (Segarra et al., 2015) which could account

for the high S-AOM contribution to AOM at Station NP1. Nevertheless, a higher S-AOM contribution in a low-brackish station than in mid/high-brackish and marine stations remains surprising.

Notably, sampling took place during low tide, potentially capturing a snapshot of salinity and sulfate concentrations at their lowest. Over a full tidal cycle these concentrations likely vary: at high tide, tidal input supplies salinity and sulfate to all stations, whereas at low tide, drainage input dilutes salinity and sulfate most strongly at nitrogen-polluted stations. Salinity and sulfate concentrations may therefore span overlapping ranges across the stations, so S-AOM contributions should be compared across those ranges rather than low tide values. This likely does not apply to Station X which experienced very low to no nitrogen pollution (see section 4.1). It remains surprising that S-AOM was not detected at Station X but was detected at the stations with lower salinities and sulfate concentrations.

One possibility is that high rates of organic matter degradation inhibited S-AOM (Lapham et al., 2024). Organic matter degradation can generate hydrogen through fermentation (Lovley et al., 1982) and drive hydrogenotrophic sulfate reduction. Hydrogenotrophic sulfate reduction is more energetically favorable than S-AOM and thus may outcompete AOM for sulfate (Jørgensen et al., 2019; Thauer et al., 1977) (see also Table 1). Furthermore, the energetic feasibility of AOM decreases with increasing hydrogen concentrations (> 0.3 nM) (Hoehler et al., 1994, 1998). AOM rates at Station X (N-Starved incubations) were significantly lower than AOM rates in all other stations ($p < 0.05$), potentially indicating relatively increased presence of suppressing agents, such as hydrogen. It should also be noted that high organic carbon, specifically humic substances, may stimulate N/S-independent AOM (Valenzuela et al., 2017). Therefore, while S-AOM may have been inhibited, N/S-independent AOM may have persisted despite elevated

hydrogen concentrations due to the availability of humic substances as alternative electron acceptors.

Alternatively, the calculated S-AOM and N/S-independent AOM contributions may carry methodological bias. Molybdate treatment was used to exclude S-AOM by inhibiting sulfate reduction, but this assumes that distinct microbial populations conduct S-AOM and N/S-independent AOM. It is possible that microbes implicated in both S-AOM and N/S-independent AOM (e.g. ANME-2a/2c) (Scheller et al., 2016) switched between electron acceptors depending upon availability, including switching from S-AOM to N/S-independent AOM in molybdate-treated incubations. Thus, the N/S-independent AOM contributions would be artificially increased. This artificial increase would be surprising as it would indicate that some microbes conducting S-AOM while sulfate is available are also capable of conducting the more energetically favorable N/S-independent AOM yet do not until sulfate reduction is inhibited. One potential explanation is that more-crystalline iron oxides can facilitate sulfate reduction (and S-AOM) over iron reduction (and iron-dependent AOM), even in sediment rich in microbially reducible iron(III) (Hansel et al., 2015). Accordingly, the molybdate-treated incubations may reveal the metabolic versatility of AOM-conducting microbial communities across the stations. Versatility would be highest at Station X where AOM switched readily to N/S-independent AOM when sulfate reduction was inhibited (Fig. 6). Versatility would be lowest at Station NP1 as sulfate reduction inhibition considerably reduced AOM rates, and intermediate at Stations NP2 and NP3. Differences in the abundances of such versatile microbes (e.g. ANME-2a/2c), may have influenced S-AOM contributions among the stations.

Collectively, these findings suggest that, in coastal wetland sediments (0–3 cm), higher porewater salinity and sulfate concentrations may not correlate with higher S-AOM contributions

and may not indicate that sulfate reduction is the primary driver of AOM. Potentially, tidal and freshwater input regularly supply and dilute porewater salinity and sulfate concentrations, obscuring sulfate availability for AOM. Additionally, high rates of organic matter degradation and the metabolic versatility of AOM-conducting microbes may influence the relative contributions of S-AOM and N/S-independent AOM to total AOM. The combination of these factors may produce the atypical relationship between S-AOM contributions to AOM, and salinity and sulfate concentrations observed in this study.

4.4.2 Prominent N/S-independent AOM in marine sediment slurry incubations

N/S-independent AOM accounted for up to 100% of AOM at Station X (Figs. 6, 7). The expected response of N/S-independent AOM rates to molybdate treatment, a competitive sulfate reduction inhibitor, is no change (Hansen et al., 1998; Liu et al., 2025). However, Station X AOM rates significantly increased with molybdate treatment (Fig. 6). One study, which also observed molybdate-stimulated AOM rates under marine conditions, proposed that S-AOM inhibition may increase the energetic favorability of AOM coupled to other electron acceptors (van Grinsven et al., 2020). Furthermore, molybdate may also influence microbial methanogenesis. Sulfate reduction typically outcompetes methanogenesis for competitive substrates (e.g. hydrogen and acetate) (Jørgensen, 2000; Oremland & Polcin, 1982). The energetic favorability of sulfate reduction over methanogenesis gives sulfate reducers a higher affinity for shared substrate, resulting in sulfate reducers maintaining substrate concentrations too low for methanogenesis to be energetically favorable (Kristjansson et al., 1982). Molybdate treatment may have facilitated methanogenesis by removing its primary competitor, potentially

leading to non-competitive methane production at Station X incubations and thereby stimulating N/S-independent AOM (Hansen et al., 1998).

4.5 Humic substances stimulate AOM in the absence of classical electron acceptors

From the discussion thus far, it is evident that N/S-independent AOM is a prominent contributor to AOM at all stations, particularly under nitrate-amended conditions. Another goal in this study was to identify candidates for N/S-independent AOM, specifically if humic substances were available for AOM. Humic substances are naturally occurring and redox-available organic carbon compounds (Lovley et al., 1996). Humics-AOM can occur in sediment with varying salinities, including methane seep sediment (Scheller et al., 2016), a freshwater bioreactor (Bai et al., 2019), a brackish tropical wetland (Valenzuela et al., 2017, 2019), and paddy soil (Fan et al., 2020). High substrate concentrations (high organic carbon content) can stimulate humics-AOM (Valenzuela et al., 2017). Previous work at Station NP3 identified that sediment total organic carbon concentrations were highest within the top 2.5 cm (Krause et al., 2025). It is therefore plausible that humics-AOM contributed to N/S-independent AOM in Station NP3 incubations (0–3 cm).

Humics-AOM rates were determined at Station NP3 by comparing AOM rates in AQDS-treated incubations (+ AQDS and + Mb + S + AQDS) and control treatments (N-Starved and + Mb + S) where the difference was assumed to be humics-AOM. Humics-AOM was not detectable in AQDS-treated incubations with active iron and sulfate reduction (Fig. 8A). However, when iron-dependent AOM and S-AOM were inhibited, humics-AOM was detected in AQDS-treated incubations. Detection solely in inhibitory treatments may suggest that microbes capable of humics-AOM are present but may be conducting iron-dependent AOM or S-AOM

under typical environmental conditions. Candidates for humics-AOM include ANME-2c (Scheller et al., 2016), an ANME lineage detected at Station NP3 (Krause et al., 2025) which can also conduct iron-dependent AOM (Xiao et al., 2023) and S-AOM (Knittel & Boetius, 2009; Timmers et al., 2017). Humics-AOM is less energetically favorable than iron-dependent AOM but more favorable than S-AOM at standard conditions (Table 1). In situ thermodynamics — resulting from environmental concentrations of electron acceptors, donors, and products (Knittel & Boetius, 2009) — may have shifted the relative favorability of both iron-dependent AOM and S-AOM to be higher than humics-AOM. We suggest that microbes capable of humics-dependent AOM are present at Station NP3 and that humics-AOM may contribute to present N/S-independent AOM. However, under typical environmental conditions, iron-dependent AOM and S-AOM are likely the dominant AOM pathways. It is possible that humics-AOM at Station NP3 may be attributed to ANME-2c; however, other microbial lineages not previously detected could also be involved.

Notably, AOM persisted even in incubations where sulfate and iron reduction were inhibited and no AQDS was added (Fig. 8A) which may be attributed to less reactive humic substances already present in the incubation sediment. Sulfide treatment was used to remove microbially reducible iron(III) from potential iron reduction and may have also removed highly reactive humic substances from potential microbial reduction. It is plausible that sulfide treatment did not remove less reactive humic substances from potential microbial reduction and that these less reactive humic substances were available for humics-AOM.

4.6 Methane-derived dissolved organic carbon production linked to anaerobic methanotrophy

Aerobic methane-oxidizing bacteria (Hanson & Hanson, 1996) and ANME (Boetius et al., 2000; Knittel & Boetius, 2009; Wegener et al., 2008) are known to oxidize methane into inorganic carbon and fix methane into their biomass. Furthermore, recent studies have shown that some aerobic methane-oxidizing bacteria (Gilman et al., 2017; Kalyuzhnaya et al., 2013; Schorn et al., 2024), NC10 bacteria (H. Chen et al., 2018, 2019), and ANME (S. Yang et al., 2020) may produce DOC (including formate, acetate, and lactate) derived directly from methane under oxygen-limited conditions. This direct methane-derived DOC production is still poorly understood and has only been shown to occur in freshwater lakes (aerobic methane-oxidizing bacteria) (Schorn et al., 2024) and bioreactor cultures (aerobic methane-oxidizing bacteria, NC10, ANME) (H. Chen et al., 2018, 2019; Gilman et al., 2017; Kalyuzhnaya et al., 2013; S. Yang et al., 2020). More classically, methane-derived DOC may be produced indirectly from methane-derived DIC and biomass (Lalk et al., 2025; Pohlman et al., 2011). This indirect methane-derived DOC production is typically ascribed to methane seep environments where methane is a dominant component within the carbon cycle and can contribute greatly to the DOC pool (Pohlman et al., 2011). Alternatively, a recent study found that ANME-2d can indirectly produce acetate from methane-derived intracellular compounds (Cai et al., 2019). Direct and indirect methane-derived DOC production may be difficult to differentiate, but cumulative methane-derived DOC production may be an underrecognized aspect of the carbon cycle in which methane-derived DOC contributes to heterotrophy (Oshkin et al., 2015; Radajewski et al., 2003).

Methane-derived DOC was extracted according to the methods outlined in section 2.4.5. DIC was removed with acidification, while biomass was removed with filtration (0.22 μm, polyethersulfone). Additionally, methane-derived biomass was unlikely to have accumulated due

to the slow (several months) doubling time of ANME (Girguis et al., 2005; Meulepas et al., 2009; Nauhaus et al., 2007). Methane-derived DOC production was detected in all live Station NP3 incubations at 0–21 pmol cm^{-3} d^{-1}, around one to two orders of magnitude lower than AOM (Fig. 8B). Methane-derived DOC production was primarily attributed to ANME or canonical methanogens (see section 3.2.4) as BES treatment significantly suppressed methane-derived DOC production, indicating that methyl-coenzyme M reductase was involved in methane-derived DOC production. Methane-derived DOC production may potentially be attributed to ANME-2c, previously detected at Station NP3 (Krause et al., 2025), though it is important to note that other microbes may also have been involved. There was no evidence for methane-derived DOC production linked to aerobic methanotrophy: inhibitory agents for aerobic methanotrophy did not significantly affect methane-derived DOC production relative to BES treatment.

Methane-derived DOC production significantly increased when iron and sulfate reduction were inhibited relative to the N-Starved treatment, plausibly because DOC consumption (including methane-derived DOC) linked to organoclastic iron and sulfate reduction was inhibited. Methane-derived DOC production also significantly increased with AQDS treatment alone, potentially indicating the involvement of AQDS in the metabolic process (Fig. 8B). Since electron acceptors may be necessary to activate methane for DOC production (H. Chen et al., 2019) AQDS may have facilitated methane activation for methane-derived DOC production.

It is, however, unlikely that AQDS stimulated indirect methane-derived DOC production. Indirect methane-derived DOC production could plausibly be fueled by increased DIC or biomass production from AOM. But AQDS treatment alone did not stimulate AOM (Fig. 8A). Conversely, AQDS treatment could have fueled DOC and biomass consumption as AQDS is a

potential electron acceptor for organic matter degradation (Lovley et al., 1996). Furthermore, relatively low rates of methane-derived DIC production via AOM (~0.3 nmol cm^{-3} bulk sediment d^{-1}) were likely diluted by incubation media DIC concentrations (~400,000 nmol bicarbonate) (Laso-Pérez et al., 2018). Rather, it is feasible that AQDS stimulated methane activation for direct methane-derived DOC production. We therefore propose that humic substances were more likely involved in direct methane-derived DOC production and that direct methane-derived DOC production may have been active at Station NP3. Similarly, in incubations where iron and sulfate reduction were inhibited but no AQDS was added (+ Mb + S), increased methane-derived DOC production may partially be attributed less reactive humic substances (not removed by sulfide) stimulating direct methane-derived DOC production (Fig. 8B). Increased methane-derived DOC production in + Mb + S incubations may also be partially attributed to inhibited DOC consumption via organoclastic iron and sulfate reduction.

These findings extend previous observations from bioreactors of methane-derived DOC production linked to ANME to sediment slurry incubations with coastal wetland sediments (S. Yang et al., 2020). Furthermore, these findings propose a previously unexplored electron acceptor potentially involved in direct methane-derived DOC production, humic substances (S. Yang et al., 2020).

5. Conclusion

This study from CSMR demonstrates the effects of simulated nitrate pollution on various AOM pathways (N-AOM, S-AOM, and N/S-independent AOM) as well as total AOM in coastal wetland sediments (Fig. 9). The prominent impact of nitrate amendment was suppressed S-AOM and decreased total AOM rates across the nitrogen-polluted stations (Stations NP1, NP2, and NP3), while N-AOM was a relatively minor contributor to AOM that did not compensate for suppressed S-AOM. N/S-independent AOM was nitrate tolerant and a prominent contributor to total AOM, particularly under nitrate-amended conditions. Though previous works have suggested that S-AOM is the dominant contributor to AOM in coastal wetland sediments (Gao et al., 2022; La et al., 2022; Segarra et al., 2013), we observed that N/S-independent AOM was dominant over S-AOM in all nitrate-amended sediment slurry incubations across a sulfate-salinity gradient: low-brackish, mid-brackish, high-brackish, and marine. We conclude that N/S-independent AOM may represent an increasingly important contributor to AOM in nitrate-polluted coastal wetland sediments as pollution intensifies (Galloway et al., 2003, 2008; Howarth et al., 1996; Kintisch, 2013; Smith et al., 1999), particularly near the surface where maximal nitrate pollution and penetration into sediment transpires. Humics-AOM, detected at Station NP3 in the absence of classical electron acceptors, is a candidate for N/S-independent AOM. Furthermore, humic substances were suggested to stimulate methane-derived DOC production, illuminating a potentially underrecognized pathway within wetland carbon cycling.

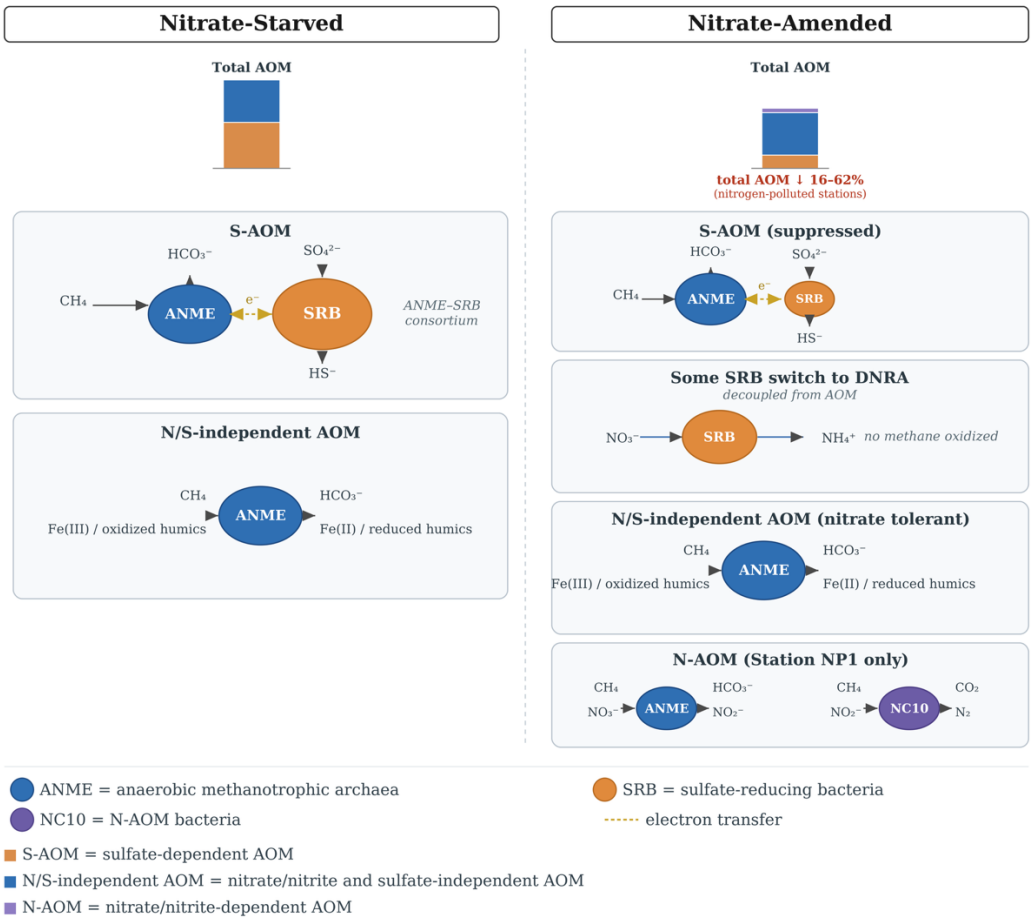

Figure 9. Illustrated responses of total AOM and its constituent pathways to nitrate amendment. On the left column, total AOM under nitrate-starved conditions is shown as well as constituent AOM pathways: S-AOM is depicted in orange; N/S-independent AOM is depicted in blue. Microbes conducting S-AOM and N/S-independent AOM under nitrate-starved conditions are shown beneath. Sulfate-reducing bacteria are shown in orange; ANME are shown in blue; electron transfer between ANME and sulfate-reducing bacteria is shown as a dashed yellow line. On the right column, total AOM under nitrate-amended conditions is shown as well as constituent AOM pathways: S-AOM is depicted in orange; N/S-independent AOM is depicted in blue; and N-AOM is depicted in purple. Microbes conducting S-AOM, N/S-independent AOM, and N-AOM under nitrate-amended conditions are shown beneath. NC10 bacteria are shown in

purple. S-AOM suppression is depicted with a relatively smaller sulfate-reducing bacterial population as well as some sulfate-reducing bacteria switching to DNRA with no methane oxidized. Nitrate tolerance in N/S-independent AOM is depicted as no change relative to nitrate-starved conditions.

Several open questions remain from this study:

(1) How sulfate-reducing microbes involved in S-AOM respond to nitrate amendment remains speculative. Metagenomic and transcriptomic analyses targeting ANME-associated sulfate-reducing bacteria could test whether nitrate amendment induces sulfate-reducing bacteria to switch to DNRA, decoupling their metabolism from AOM. Furthermore, dose-response experiments could evaluate a potential nitrate concentration threshold at which S-AOM suppression begins.

(2) The nitrate tolerance of individual N/S-independent AOM pathways — e.g. iron(III), manganese(IV), and humic substances — was not tested. Future works could implement specific inhibitors (if available) or culture experiments to isolate individual N/S-independent AOM pathways and assess if their nitrate tolerance differs.

(3) It is further not clear which variables control the relative contributions of N/S-independent AOM and S-AOM to total AOM in coastal wetland sediments. S-AOM and N/S-independent AOM contributions should be tested under different conditions: stage in tidal cycle, sediment depth, sediment type, biogeochemical characteristics not tested in this study (e.g. pH).

(4) Methane-derived DOC production in coastal wetland sediments is still not well understood. Future studies should characterize the importance of methane-derived DOC

production across horizontal and vertical sediment distributions and the microbial lineages putatively involved.

Appendix

Table 4. Water column and sediment porewater unaggregated data. Station ID and sampling date for Carpinteria Salt Marsh Reserve water column and drainage water samples, and sediment cores, with nitrite, nitrate, ammonium, methane, salinity, and sulfate reported by sediment depth. "-" = not measured.

Station ID	Sampling Date	Sediment depth (cm)	Nitrite (µM)	Nitrate (µM)	Ammonium (µM)	Methane (µM)	Sulfate (mM)	Salinity (g kg^{-1})
Station NP1	06/17/2025	drainage	5.7	2095	0	-	-	-
Station NP1	06/17/2025	supernatant	19	978	0	-	2.5	2.2
Station NP1	06/17/2025	water column	3.9	1903	0	-	1.8	1.1
Station NP1	06/17/2025	0.5	0.0	0.0	164	3.5	3.5	3.9
Station NP1	06/17/2025	1.5	0.0	2.0	152	0.9	4.8	5.1
Station NP1	06/17/2025	2.5	1.2	1.3	71	1.0	6.8	7.6
Station NP1	06/17/2025	3.5	3.7	3.9	-	-	-	-
Station NP2	08/12/2024	supernatant	20	117	14	0.0	1.0	2.0
Station NP2	08/12/2024	water column	1.8	188	3.4	0.0	0.0	0.0
Station NP2	08/12/2024	0.5	0.0	0.7	137	8.4	11	10
Station NP2	08/12/2024	1.5	0.0	1.2	125	8.7	14	13
Station NP2	08/12/2024	2.5	0.0	0.8	119	9.1	14	16
Station NP2	08/12/2024	3.5	0.0	0.8	100	6.3	-	-
Station NP2	08/12/2024	4.5	0.0	0.0	105	-	-	-
Station NP2	08/12/2024	6.5	0.0	0.9	135	-	-	-
Station NP2	08/12/2024	7.5	0.0	1.2	143	-	-	-
Station NP2	08/12/2024	8.5	0.0	1.1	199	-	-	-
Station NP2	08/12/2024	9.5	0.0	0.9	253	-	-	-
Station NP2	08/12/2024	11.0	0.0	1.6	273	-	-	-

Station ID	Sampling Date	Sediment depth (cm)	Nitrite (µM)	Nitrate (µM)	Ammonium (µM)	Methane (µM)	Sulfate (mM)	Salinity (g kg^{-1})
Station NP2	08/12/2024	12.0	0.0	9.4	295	-	-	-
Station NP2	08/12/2024	15.0	0.0	6.9	286	-	-	-
Station NP2	08/12/2024	17.0	0.0	4.7	288	-	-	-
Station NP2	08/12/2024	19.0	0.0	3.9	285	-	-	-
Station NP2	08/12/2024	21.0	0.0	3.1	277	-	-	-
Station NP2	06/17/2025	drainage	1.3	409	0	-	-	-
Station NP2	06/17/2025	supernatant	2.2	28	0	-	8.1	11
Station NP2	06/17/2025	water column	2.7	311	0	-	7.9	10
Station NP2	06/17/2025	0.2	-	-	-	-	15	20
Station NP2	06/17/2025	0.5	0.0	0.6	0	-	-	-
Station NP2	06/17/2025	0.8	-	-	-	-	15	19
Station NP2	06/17/2025	1.5	0.0	5.9	227	4.9	15	21
Station NP2	06/17/2025	2.5	0.0	5.6	244	7.2	15	21
Station NP2	06/17/2025	3.5	0.0	4.9	-	5.1	-	-
Station NP3	06/17/2025	supernatant	1.6	140	0	-	14	18
Station NP3	06/17/2025	water column	2.5	199	0	-	13	18
Station NP3	06/17/2025	0.5	0.0	0.0	8.0	2.0	20	27
Station NP3	06/17/2025	1.5	0.0	0.5	285	2.2	21	27
Station NP3	06/17/2025	2.5	0.0	0.5	388	2.0	24	30
Station NP3	06/17/2025	3.5	0.0	-	-	1.8	-	-
Station NP3	08/27/2025	supernatant	5.9	72	4.0	-	11	17
Station NP3	08/27/2025	water column	0.0	95	2.0	-	8.0	17
Station NP3	08/27/2025	0.5	0.0	1.9	77	3.0	20	25
Station NP3	08/27/2025	1.5	0.0	0.5	135	3.1	21	28
Station NP3	08/27/2025	2.5	0.0	0.5	158	2.1	22	29
Station NP3	08/27/2025	3.5	0.0	-	167	3.5	25	35

Station ID	Sampling Date	Sediment depth (cm)	Nitrite (µM)	Nitrate (µM)	Ammonium (µM)	Methane (µM)	Sulfate (mM)	Salinity (g kg^{-1})
Station X	06/17/2025	supernatant	0.0	18	0	-	27	34
Station X	06/17/2025	water column	0.0	4.4	0	-	27	35
Station X	06/17/2025	0.5	0.0	0.0	-	4.7	27	36
Station X	06/17/2025	1.5	0.0	0.0	71	4.6	27	36
Station X	06/17/2025	2.5	0.0	0.0	-	3.8	26	36

Table 5. Potential sulfate reduction rate unaggregated data in Station NP2 sediment slurry incubations.

Station ID	Sampling Date	Nitrate (µM)	Treatment	Sulfate Reduction Rate (nmol cm^{-3} d^{-1})
Station NP2	08/12/2024	8	N_2	272
Station NP2	08/12/2024	8	N_2	317
Station NP2	08/12/2024	8	N_2	283
Station NP2	08/12/2024	8	$N_2 + CH_4$	253
Station NP2	08/12/2024	8	$N_2 + CH_4$	311
Station NP2	08/12/2024	8	$N_2 + CH_4$	259
Station NP2	08/12/2024	803	N_2	203
Station NP2	08/12/2024	803	N_2	134
Station NP2	08/12/2024	803	N_2	197
Station NP2	08/12/2024	803	$N_2 + CH_4$	248
Station NP2	08/12/2024	803	$N_2 + CH_4$	242
Station NP2	08/12/2024	803	$N_2 + CH_4$	201

Table 6. $^{15}NO_3^-$ consumption over time unaggregated data in Station NP2 sediment slurry incubations.

Process	Sampling Date	Treatment	Incubation time (days)	Product produced (µmol)	$^{15}NO_3^-$ consumed (µmol)
Denitrification	08/12/2024	N_2	0.00	$^{30}N_2$ 0.00	0.00
Denitrification	08/12/2024	N_2	0.00	$^{30}N_2$ 0.00	0.00
Denitrification	08/12/2024	N_2	0.00	$^{30}N_2$ 0.00	0.00
Denitrification	08/12/2024	N_2	0.29	$^{30}N_2$ 1.25	2.51
Denitrification	08/12/2024	N_2	0.29	$^{30}N_2$ 1.49	2.99
Denitrification	08/12/2024	N_2	0.29	$^{30}N_2$ 1.16	2.32
Denitrification	08/12/2024	N_2	0.75	$^{30}N_2$ 4.13	8.26
Denitrification	08/12/2024	N_2	0.75	$^{30}N_2$ 3.76	7.53
Denitrification	08/12/2024	N_2	0.75	$^{30}N_2$ 5.18	10.35
Denitrification	08/12/2024	N_2	1.00	$^{30}N_2$ 5.68	11.35
Denitrification	08/12/2024	N_2	1.00	$^{30}N_2$ 6.07	12.14
Denitrification	08/12/2024	N_2	1.00	$^{30}N_2$ 5.95	11.91
Denitrification	08/12/2024	$N_2 + CH_4$	0.00	$^{30}N_2$ 0.00	0.00
Denitrification	08/12/2024	$N_2 + CH_4$	0.00	$^{30}N_2$ 0.00	0.00
Denitrification	08/12/2024	$N_2 + CH_4$	0.00	$^{30}N_2$ 0.00	0.00
Denitrification	08/12/2024	$N_2 + CH_4$	0.29	$^{30}N_2$ 1.71	3.42

Process	Sampling Date	Treatment	Incubation time (days)	Product produced (µmol)	$^{15}NO_3^-$ consumed (µmol)
Denitrification	08/12/2024	$N_2 + CH_4$	0.29	$^{30}N_2$ 1.85	3.70
Denitrification	08/12/2024	$N_2 + CH_4$	0.29	$^{30}N_2$ 1.78	3.56
Denitrification	08/12/2024	$N_2 + CH_4$	0.75	$^{30}N_2$ 4.02	8.04
Denitrification	08/12/2024	$N_2 + CH_4$	0.75	$^{30}N_2$ 5.69	11.38
Denitrification	08/12/2024	$N_2 + CH_4$	0.75	$^{30}N_2$ 4.79	9.59
Denitrification	08/12/2024	$N_2 + CH_4$	1.00	$^{30}N_2$ 6.15	12.29
Denitrification	08/12/2024	$N_2 + CH_4$	1.00	$^{30}N_2$ 6.75	13.49
Denitrification	08/12/2024	$N_2 + CH_4$	1.00	$^{30}N_2$ 6.88	13.76
DNRA	08/12/2024	N_2	0.00	$^{15}NH_4^+$ 0.00	0.00
DNRA	08/12/2024	N_2	0.00	$^{15}NH_4^+$ 0.00	0.00
DNRA	08/12/2024	N_2	0.00	$^{15}NH_4^+$ 0.00	0.00
DNRA	08/12/2024	N_2	0.29	$^{15}NH_4^+$ 3.62	3.62
DNRA	08/12/2024	N_2	0.29	$^{15}NH_4^+$ 5.45	5.45
DNRA	08/12/2024	N_2	0.29	$^{15}NH_4^+$ 3.95	3.95
DNRA	08/12/2024	N_2	0.75	$^{15}NH_4^+$ 10.17	10.17
DNRA	08/12/2024	N_2	0.75	$^{15}NH_4^+$ 8.80	8.80
DNRA	08/12/2024	N_2	0.75	$^{15}NH_4^+$ 10.30	10.30
DNRA	08/12/2024	N_2	1.00	$^{15}NH_4^+$ 10.20	10.20

Process	Sampling Date	Treatment	Incubation time (days)	Product produced (µmol)	$^{15}NO_3^-$ consumed (µmol)
DNRA	08/12/2024	N_2	1.00	$^{15}NH_4^+$ 8.44	8.44
DNRA	08/12/2024	N_2	1.00	$^{15}NH_4^+$ 12.13	12.13
DNRA	08/12/2024	$N_2 + CH_4$	0.00	$^{15}NH_4^+$ 0.00	0.00
DNRA	08/12/2024	$N_2 + CH_4$	0.00	$^{15}NH_4^+$ 0.00	0.00
DNRA	08/12/2024	$N_2 + CH_4$	0.00	$^{15}NH_4^+$ 0.00	0.00
DNRA	08/12/2024	$N_2 + CH_4$	0.29	$^{15}NH_4^+$ 7.14	7.14
DNRA	08/12/2024	$N_2 + CH_4$	0.29	$^{15}NH_4^+$ 5.03	5.03
DNRA	08/12/2024	$N_2 + CH_4$	0.29	$^{15}NH_4^+$ 4.66	4.66
DNRA	08/12/2024	$N_2 + CH_4$	0.75	$^{15}NH_4^+$ 11.79	11.79
DNRA	08/12/2024	$N_2 + CH_4$	0.75	$^{15}NH_4^+$ 11.79	11.79
DNRA	08/12/2024	$N_2 + CH_4$	0.75	$^{15}NH_4^+$ 10.05	10.05
DNRA	08/12/2024	$N_2 + CH_4$	1.00	$^{15}NH_4^+$ 11.78	11.78
DNRA	08/12/2024	$N_2 + CH_4$	1.00	$^{15}NH_4^+$ 9.57	9.57
Anammox	08/12/2024	N_2	0.00	$^{29}N_2$ 0.00	0.00
Anammox	08/12/2024	N_2	0.00	$^{29}N_2$ 0.00	0.00
Anammox	08/12/2024	N_2	0.00	$^{29}N_2$ 0.00	0.00
Anammox	08/12/2024	N_2	0.29	$^{29}N_2$ 0.19	0.19
Anammox	08/12/2024	N_2	0.29	$^{29}N_2$ 0.17	0.17

Process	Sampling Date	Treatment	Incubation time (days)	Product produced (µmol)	$^{15}NO_3^-$ consumed (µmol)
Anammox	08/12/2024	N_2	0.29	$^{29}N_2$ 0.15	0.15
Anammox	08/12/2024	N_2	0.75	$^{29}N_2$ 0.25	0.25
Anammox	08/12/2024	N_2	0.75	$^{29}N_2$ 0.23	0.23
Anammox	08/12/2024	N_2	0.75	$^{29}N_2$ 0.30	0.30
Anammox	08/12/2024	N_2	1.00	$^{29}N_2$ 0.32	0.32
Anammox	08/12/2024	N_2	1.00	$^{29}N_2$ 0.33	0.33
Anammox	08/12/2024	N_2	1.00	$^{29}N_2$ 0.34	0.34
Anammox	08/12/2024	$N_2 + CH_4$	0.00	$^{29}N_2$ 0.00	0.00
Anammox	08/12/2024	$N_2 + CH_4$	0.00	$^{29}N_2$ 0.00	0.00
Anammox	08/12/2024	$N_2 + CH_4$	0.00	$^{29}N_2$ 0.00	0.00
Anammox	08/12/2024	$N_2 + CH_4$	0.29	$^{29}N_2$ 0.15	0.15
Anammox	08/12/2024	$N_2 + CH_4$	0.29	$^{29}N_2$ 0.15	0.15
Anammox	08/12/2024	$N_2 + CH_4$	0.29	$^{29}N_2$ 0.18	0.18
Anammox	08/12/2024	$N_2 + CH_4$	0.75	$^{29}N_2$ 0.23	0.23
Anammox	08/12/2024	$N_2 + CH_4$	0.75	$^{29}N_2$ 0.35	0.35
Anammox	08/12/2024	$N_2 + CH_4$	0.75	$^{29}N_2$ 0.30	0.30
Anammox	08/12/2024	$N_2 + CH_4$	1.00	$^{29}N_2$ 0.34	0.34
Anammox	08/12/2024	$N_2 + CH_4$	1.00	$^{29}N_2$ 0.40	0.40

Process	Sampling Date	Treatment	Incubation time (days)	Product produced (µmol)	$^{15}NO_3^-$ consumed (µmol)
Anammox	08/12/2024	$N_2 + CH_4$	1.00	$^{29}N_2$ 0.39	0.39

Table 7. Potential AOM rate unaggregated data in Station NP1, NP2, NP3, and X sediment slurry incubations.

Station	Sampling Date	Treatment	AOM rate (nmol cm^{-3} d^{-1})
Station NP1	06/17/2025	N-Starved	4.66
Station NP1	06/17/2025	N-Starved	1.26
Station NP1	06/17/2025	N-Starved	1.15
Station NP1	06/17/2025	N-Starved + Mb	0.31
Station NP1	06/17/2025	N-Starved + Mb	0.48
Station NP1	06/17/2025	N-Starved + Mb	0.36
Station NP1	06/17/2025	N-Amended	0.87
Station NP1	06/17/2025	N-Amended	0.91
Station NP1	06/17/2025	N-Amended	0.88
Station NP1	06/17/2025	N-Amended + Mb	0.52
Station NP1	06/17/2025	N-Amended + Mb	0.52
Station NP1	06/17/2025	N-Amended + Mb	0.55
Station NP2	06/17/2025	N-Starved	0.99
Station NP2	06/17/2025	N-Starved	1.02
Station NP2	06/17/2025	N-Starved	1.22
Station NP2	06/17/2025	N-Starved + Mb	0.91
Station NP2	06/17/2025	N-Starved + Mb	0.63

Station	Sampling Date	Treatment	AOM rate (nmol cm^{-3} d^{-1})
Station NP2	06/17/2025	N-Starved + Mb	0.65
Station NP2	06/17/2025	N-Amended	0.75
Station NP2	06/17/2025	N-Amended	0.68
Station NP2	06/17/2025	N-Amended	0.83
Station NP2	06/17/2025	N-Amended + Mb	0.73
Station NP2	06/17/2025	N-Amended + Mb	0.69
Station NP2	06/17/2025	N-Amended + Mb	0.92
Station NP3	06/17/2025	N-Starved	0.99
Station NP3	06/17/2025	N-Starved	1.09
Station NP3	06/17/2025	N-Starved	1.04
Station NP3	06/17/2025	N-Starved + Mb	0.73
Station NP3	06/17/2025	N-Starved + Mb	0.57
Station NP3	06/17/2025	N-Starved + Mb	0.47
Station NP3	06/17/2025	N-Amended	0.86
Station NP3	06/17/2025	N-Amended	0.85
Station NP3	06/17/2025	N-Amended	0.92
Station NP3	06/17/2025	N-Amended + Mb	0.65
Station NP3	06/17/2025	N-Amended + Mb	0.69
Station NP3	06/17/2025	N-Amended + Mb	0.79

Station	Sampling Date	Treatment	AOM rate (nmol cm^{-3} d^{-1})
Station X	06/17/2025	N-Starved	0.34
Station X	06/17/2025	N-Starved	0.25
Station X	06/17/2025	N-Starved	0.32
Station X	06/17/2025	N-Starved + Mb	0.42
Station X	06/17/2025	N-Starved + Mb	0.67
Station X	06/17/2025	N-Starved + Mb	0.64
Station X	06/17/2025	N-Amended	0.33
Station X	06/17/2025	N-Amended	0.31
Station X	06/17/2025	N-Amended	0.16
Station X	06/17/2025	N-Amended + Mb	0.48
Station X	06/17/2025	N-Amended + Mb	0.36
Station X	06/17/2025	N-Amended + Mb	0.66

Table 8. Potential AOM and CH_4-derived DOC production rate unaggregated data in Station NP3 sediment slurry incubations.

Station	Sampling Date	Treatment	AOM rate (nmol cm^{-3} d^{-1})	Methane-derived DOC production (pmol cm^{-3} d^{-1})
Station NP3	08/27/2025	N-Starved	0.28	4.4
Station NP3	08/27/2025	N-Starved	0.28	5.0
Station NP3	08/27/2025	N-Starved	0.25	4.9
Station NP3	08/27/2025	+ AQDS	0.25	14.3
Station NP3	08/27/2025	+ AQDS	0.18	12.7
Station NP3	08/27/2025	+ AQDS	0.25	13.0
Station NP3	08/27/2025	+ Mb + S	0.19	21.1
Station NP3	08/27/2025	+ Mb + S	0.16	17.6
Station NP3	08/27/2025	+ Mb + S	0.19	18.0
Station NP3	08/27/2025	+ Mb + S + AQDS	0.37	13.8
Station NP3	08/27/2025	+ Mb + S + AQDS	0.34	15.4
Station NP3	08/27/2025	+ Mb + S + AQDS	0.38	16.8
Station NP3	08/27/2025	+ Mb + S + BES	0.05	2.9
Station NP3	08/27/2025	+ Mb + S + BES	0.04	1.3
Station NP3	08/27/2025	+ Mb + S + BES	0.06	2.0

Station	Sampling Date	Treatment	AOM rate (nmol cm^{-3} d^{-1})	Methane-derived DOC production (pmol cm^{-3} d^{-1})
Station NP3	08/27/2025	+ Mb + S + BES + O	0.05	0.9
Station NP3	08/27/2025	+ Mb + S + BES + O	0.05	0.0
Station NP3	08/27/2025	+ Mb + S + BES + O	0.05	1.7
Station NP3	08/27/2025	+ Mb + S + BES + ANTI	0.06	0.0
Station NP3	08/27/2025	+ Mb + S + BES + ANTI	0.05	0.0
Station NP3	08/27/2025	+ Mb + S + BES + ANTI	0.05	1.6

References

Aromokeye, D. A., Kulkarni, A. C., Elvert, M., Wegener, G., Henkel, S., Coffinet, S., Eickhorst, T., Oni, O. E., Richter-Heitmann, T., Schnakenberg, A., Taubner, H., Wunder, L., Yin, X., Zhu, Q., Hinrichs, K.-U., Kasten, S., & Friedrich, M. W. (2020). Rates and Microbial Players of Iron-Driven Anaerobic Oxidation of Methane in Methanic Marine Sediments. Frontiers in Microbiology, 10. https://doi.org/10.3389/fmicb.2019.03041

Bai, Y.-N., Wang, X.-N., Wu, J., Lu, Y.-Z., Fu, L., Zhang, F., Lau, T.-C., & Zeng, R. J. (2019). Humic substances as electron acceptors for anaerobic oxidation of methane driven by ANME-2d. Water Research, 164, 114935. https://doi.org/10.1016/j.watres.2019.114935

Baker, L. A. (1992). Introduction to nonpoint source pollution in the United States and prospects for wetland use. Ecological Engineering, 1(1), 1–26. https://doi.org/10.1016/0925-8574(92)90023-U

Beal, E. J., House, C. H., & Orphan, V. J. (2009). Manganese- and Iron-Dependent Marine Methane Oxidation. Science, 325(5937), 184–187. https://doi.org/10.1126/science.1169984

Boetius, A., Ravenschlag, K., Schubert, C. J., Rickert, D., Widdel, F., Gieseke, A., Amann, R., Jørgensen, B. B., Witte, U., & Pfannkuche, O. (2000). A marine microbial consortium apparently mediating anaerobic oxidation of methane. Nature, 407(6804), 623–626. https://doi.org/10.1038/35036572

Bourceau, O. M., Ferdelman, T., Lavik, G., Mussmann, M., Kuypers, M. M. M., & Marchant, H. K. (2023). Simultaneous sulfate and nitrate reduction in coastal sediments. ISME Communications, 3(1), 17. https://doi.org/10.1038/s43705-023-00222-y

Bridgham, S. D., Cadillo-Quiroz, H., Keller, J. K., & Zhuang, Q. (2013). Methane emissions from wetlands: Biogeochemical, microbial, and modeling perspectives from local to global scales. Global Change Biology, 19(5), 1325–1346. https://doi.org/10.1111/gcb.12131

Bridgham, S. D., Megonigal, J. P., Keller, J. K., Bliss, N. B., & Trettin, C. (2006). The carbon balance of North American wetlands. Wetlands, 26(4), 889–916. https://doi.org/10.1672/0277-5212(2006)26%5B889:TCBONA%5D2.0.CO;2

Buessecker, S., Tylor, K., Nye, J., Holbert, K. E., Urquiza Muñoz, J. D., Glass, J. B., Hartnett, H. E., & Cadillo-Quiroz, H. (2019). Effects of sterilization techniques on chemodenitrification and N2O production in tropical peat soil microcosms. Biogeosciences, 16(23), 4601–4612. https://doi.org/10.5194/bg-16-4601-2019

Cai, C., Shi, Y., Guo, J., Tyson, G. W., Hu, S., & Yuan, Z. (2019). Acetate Production from Anaerobic Oxidation of Methane via Intracellular Storage Compounds. Environmental Science & Technology, 53(13), 7371–7379. https://doi.org/10.1021/acs.est.9b00077

Caldwell, S. L., Laidler, J. R., Brewer, E. A., Eberly, J. O., Sandborgh, S. C., & Colwell, F. S. (2008). Anaerobic Oxidation of Methane: Mechanisms, Bioenergetics, and the Ecology of Associated Microorganisms. Environmental Science & Technology, 42(18), 6791–6799. https://doi.org/10.1021/es800120b

Canfield, D. E., Kristensen, E., & Thamdrup, B. (2005). Aquatic geomicrobiology. Advances in Marine Biology, 48, 1–599. https://doi.org/10.1016/S0065-2881(05)48017-7

Chen, F., Zheng, Y., Hou, L., Niu, Y., Gao, D., An, Z., Zhou, J., Yin, G., Dong, H., Han, P., Liang, X., & Liu, M. (2021). Microbial abundance and activity of nitrite/nitrate-dependent anaerobic methane oxidizers in estuarine and intertidal wetlands:

Heterogeneity and driving factors. Water Research, 190, 116737. https://doi.org/10.1016/j.watres.2020.116737

Chen, H., Luo, J., Liu, S., Yuan, Z., & Guo, J. (2019). Microbial Methane Conversion to Short-Chain Fatty Acids Using Various Electron Acceptors in Membrane Biofilm Reactors. Environmental Science & Technology, 53(21), 12846–12855. https://doi.org/10.1021/acs.est.8b06767

Chen, H., Zhao, L., Hu, S., Yuan, Z., & Guo, J. (2018). High-Rate Production of Short-Chain Fatty Acids from Methane in a Mixed-Culture Membrane Biofilm Reactor. Environmental Science & Technology Letters, 5(11), 662–667. https://doi.org/10.1021/acs.estlett.8b00460

Chen, L., Li, L., Zhang, S., Zhang, W., Xue, K., Wang, Y., & Dong, X. (2022). Anaerobic methane oxidation linked to Fe(III) reduction in a Candidatus Methanoperedens-enriched consortium from the cold Zoige wetland at Tibetan Plateau. Environmental Microbiology, 24(2), 614–625. https://doi.org/10.1111/1462-2920.15848

Contreras, J. A., Valenzuela, E. I., & Quijano, G. (2022). Nitrate/nitrite-dependent anaerobic oxidation of methane (N-AOM) as a technology platform for greenhouse gas abatement in wastewater treatment plants: State-of-the-art and challenges. Journal of Environmental Management, 319, 115671. https://doi.org/10.1016/j.jenvman.2022.115671

Dai, Z., Fan, Y., Li, Y., Huang, Y., Mao, X., Xiang, T., Wang, F., Yang, S., & Cao, W. (2025). Global Patterns and Environmental Drives of Nitrite/Nitrate-Dependent Anaerobic Methane Oxidation Across Natural Ecosystems. Global Change Biology, 31(7), e70350. https://doi.org/10.1111/gcb.70350

Dale, A. W., Sommer, S., Lomnitz, U., Montes, I., Treude, T., Liebetrau, V., Gier, J., Hensen, C., Dengler, M., Stolpovsky, K., Bryant, L. D., & Wallmann, K. (2015). Organic carbon production, mineralisation and preservation on the Peruvian margin. Biogeosciences, 12(5), 1537–1559. https://doi.org/10.5194/bg-12-1537-2015

Deutzmann, J. S., Stief, P., Brandes, J., & Schink, B. (2014). Anaerobic methane oxidation coupled to denitrification is the dominant methane sink in a deep lake. Proceedings of the National Academy of Sciences, 111(51), 18273–18278. https://doi.org/10.1073/pnas.1411617111

Dlugokencky, E. J., Nisbet, E. G., Fisher, R., & Lowry, D. (2011). Global atmospheric methane: Budget, changes and dangers. Philosophical Transactions of the Royal Society A: Mathematical, Physical and Engineering Sciences, 369(1943), 2058–2072. https://doi.org/10.1098/rsta.2010.0341

Egger, M., Rasigraf, O., Sapart, C. J., Jilbert, T., Jetten, M. S. M., Röckmann, T., van der Veen, C., Bândă, N., Kartal, B., Ettwig, K. F., & Slomp, C. P. (2015). Iron-Mediated Anaerobic Oxidation of Methane in Brackish Coastal Sediments. Environmental Science & Technology, 49(1), 277–283. https://doi.org/10.1021/es503663z

Ettwig, K. F., Butler, M. K., Le Paslier, D., Pelletier, E., Mangenot, S., Kuypers, M. M. M., Schreiber, F., Dutilh, B. E., Zedelius, J., de Beer, D., Gloerich, J., Wessels, H. J. C. T., van Alen, T., Luesken, F., Wu, M. L., van de Pas-Schoonen, K. T., Op den Camp, H. J. M., Janssen-Megens, E. M., Francoijs, K.-J., … Strous, M. (2010). Nitrite-driven anaerobic methane oxidation by oxygenic bacteria. Nature, 464(7288), 543–548. https://doi.org/10.1038/nature08883

Evrard, V., Glud, R. N., & Cook, P. L. M. (2013). The kinetics of denitrification in permeable sediments. Biogeochemistry, 113(1), 563–572. https://doi.org/10.1007/s10533-012-9789-x

Fan, L., Dippold, M. A., Ge, T., Wu, J., Thiel, V., Kuzyakov, Y., & Dorodnikov, M. (2020). Anaerobic oxidation of methane in paddy soil: Role of electron acceptors and fertilization in mitigating CH4 fluxes. Soil Biology and Biochemistry, 141, 107685. https://doi.org/10.1016/j.soilbio.2019.107685

Fazzolari, E., Mariotti, A., & Germon, J. C. (1990). Dissimilatory ammonia production vs. Denitrification in vitro and in inoculated agricultural soil samples. Canadian Journal of Microbiology, 36(11), 786–793. https://doi.org/10.1139/m90-135

Frank, J., Zhang, X., Marcellin, E., Yuan, Z., & Hu, S. (2023). Salinity effect on an anaerobic methane- and ammonium-oxidising consortium: Shifts in activity, morphology, osmoregulation and syntrophic relationship. Water Research, 242, 120090. https://doi.org/10.1016/j.watres.2023.120090

Friedl, J., De Rosa, D., Rowlings, D. W., Grace, P. R., Müller, C., & Scheer, C. (2018). Dissimilatory nitrate reduction to ammonium (DNRA), not denitrification dominates nitrate reduction in subtropical pasture soils upon rewetting. Soil Biology and Biochemistry, 125, 340–349. https://doi.org/10.1016/j.soilbio.2018.07.024

Froelich, P. N., Klinkhammer, G. P., Bender, M. L., Luedtke, N. A., Heath, G. R., Cullen, D., Dauphin, P., Hammond, D., Hartman, B., & Maynard, V. (1979). Early oxidation of organic matter in pelagic sediments of the eastern equatorial Atlantic: Suboxic diagenesis. Geochimica et Cosmochimica Acta, 43(7), 1075–1090. https://doi.org/10.1016/0016-7037(79)90095-4

Galloway, J. N., Aber, J. D., Erisman, J. W., Seitzinger, S. P., Howarth, R. W., Cowling, E. B., & Cosby, B. J. (2003). The Nitrogen Cascade. BioScience, 53(4), 341–356. https://doi.org/10.1641/0006-3568(2003)053%5B0341:TNC%5D2.0.CO;2

Galloway, J. N., Townsend, A. R., Erisman, J. W., Bekunda, M., Cai, Z., Freney, J. R., Martinelli, L. A., Seitzinger, S. P., & Sutton, M. A. (2008). Transformation of the nitrogen cycle: Recent trends, questions, and potential solutions. Science, 320(5878), 889–892. https://doi.org/10.1126/science.1136674

Gao, Y., Wang, Y., Lee, H.-S., & Jin, P. (2022). Significance of anaerobic oxidation of methane (AOM) in mitigating methane emission from major natural and anthropogenic sources: A review of AOM rates in recent publications. Environmental Science: Advances, 1(4), 401–425. https://doi.org/10.1039/D2VA00091A

García-Robledo, E., Corzo, A., & Papaspyrou, S. (2014). A fast and direct spectrophotometric method for the sequential determination of nitrate and nitrite at low concentrations in small volumes. Marine Chemistry, 162, 30–36. https://doi.org/10.1016/j.marchem.2014.03.002

Gardner, L. R. (2007). Role of stratigraphy in governing pore water seepage from salt marsh sediments. Water Resources Research, 43(7). https://doi.org/10.1029/2006WR005338

Gedney, N., Cox, P. M., & Huntingford, C. (2004). Climate feedback from wetland methane emissions. Geophysical Research Letters, 31(20). https://doi.org/10.1029/2004GL020919

Gilman, A., Fu, Y., Hendershott, M., Chu, F., Puri, A. W., Smith, A. L., Pesesky, M., Lieberman, R., Beck, D. A. C., & Lidstrom, M. E. (2017). Oxygen-limited metabolism in the methanotroph Methylomicrobium buryatense 5GB1C. PeerJ, 5, e3945. https://doi.org/10.7717/peerj.3945

Girguis, P. R., Cozen, A. E., & DeLong, E. F. (2005). Growth and Population Dynamics of Anaerobic Methane-Oxidizing Archaea and Sulfate-Reducing Bacteria in a Continuous-Flow Bioreactor. Applied and Environmental Microbiology, 71(7), 3725–3733. https://doi.org/10.1128/AEM.71.7.3725-3733.2005

Gómez-Gallego, T. (2022). N-damo, an opportunity to reduce methane emissions? Environmental Microbiology Reports, 14(5), 697–699. https://doi.org/10.1111/1758-2229.13114

Grasshoff, K., Kremling, K., & Ehrhardt, M. (2009). Methods of Seawater Analysis. John Wiley & Sons.

Grigoryan, A. A., Cornish, S. L., Buziak, B., Lin, S., Cavallaro, A., Arensdorf, J. J., & Voordouw, G. (2008). Competitive Oxidation of Volatile Fatty Acids by Sulfate- and Nitrate-Reducing Bacteria from an Oil Field in Argentina. Applied and Environmental Microbiology, 74(14), 4324–4335. https://doi.org/10.1128/AEM.00419-08

Handler, A. M., Suchy, A. K., & Grimm, N. B. (2022). Denitrification and DNRA in Urban Accidental Wetlands in Phoenix, Arizona. Journal of Geophysical Research: Biogeosciences, 127(2), e2021JG006552. https://doi.org/10.1029/2021JG006552

Hansel, C. M., Lentini, C. J., Tang, Y., Johnston, D. T., Wankel, S. D., & Jardine, P. M. (2015). Dominance of sulfur-fueled iron oxide reduction in low-sulfate freshwater sediments. The ISME Journal, 9(11), 2400–2412. https://doi.org/10.1038/ismej.2015.50

Hansen, L. B., Finster, K., Fossing, H., & Iversen, N. (1998). Anaerobic methane oxidation in sulfate depleted sediments: Effects of sulfate and molybdate additions. Aquatic Microbial Ecology, 14, 195–204. https://doi.org/10.3354/ame014195

Hanson, R. S., & Hanson, T. E. (1996). Methanotrophic bacteria. Microbiological Reviews, 60(2), 439–471. https://doi.org/10.1128/mr.60.2.439-471.1996

Haroon, M. F., Hu, S., Shi, Y., Imelfort, M., Keller, J., Hugenholtz, P., Yuan, Z., & Tyson, G. W. (2013). Anaerobic oxidation of methane coupled to nitrate reduction in a novel archaeal lineage. Nature, 500(7464), 567–570. https://doi.org/10.1038/nature12375

He, Z., Wang, J., Hu, J., Yu, H., Jetten, M. S. M., Liu, H., Cai, C., Liu, Y., Ren, H., Zhang, X., Hua, M., Xu, X., Zheng, P., & Hu, B. (2019). Regulation of coastal methane sinks by a structured gradient of microbial methane oxidizers. Environmental Pollution, 244, 228–237. https://doi.org/10.1016/j.envpol.2018.10.057

He, Z., Zhang, Q., Feng, Y., Luo, H., Pan, X., & Gadd, G. M. (2018). Microbiological and environmental significance of metal-dependent anaerobic oxidation of methane. Science of The Total Environment, 610–611, 759–768. https://doi.org/10.1016/j.scitotenv.2017.08.140

Hinrichs, K.-U., & Boetius, A. (2003). The Anaerobic Oxidation of Methane: New Insights in Microbial Ecology and Biogeochemistry. In G. Wefer, D. Billett, D. Hebbeln, B. B. Jørgensen, M. Schlüter, & T. C. E. van Weering (Eds.), Ocean Margin Systems (pp. 457–477). Springer. https://doi.org/10.1007/978-3-662-05127-6_28

Hoehler, T. M., Alperin, M. J., Albert, D. B., & Martens, C. S. (1994). Field and laboratory studies of methane oxidation in an anoxic marine sediment: Evidence for a methanogen-sulfate reducer consortium. Global Biogeochemical Cycles, 8(4), 451–463. https://doi.org/10.1029/94GB01800

Hoehler, T. M., Alperin, M. J., Albert, D. B., & Martens, C. S. (1998). Thermodynamic control on hydrogen concentrations in anoxic sediments. Geochimica et Cosmochimica Acta, 62(10), 1745–1756. https://doi.org/10.1016/S0016-7037(98)00106-9

Hou, L., Zheng, Y., Liu, M., Li, X., Lin, X., Yin, G., Gao, J., Deng, F., Chen, F., & Jiang, X. (2015). Anaerobic ammonium oxidation and its contribution to nitrogen removal in China's coastal wetlands. Scientific Reports, 5(1), 15621. https://doi.org/10.1038/srep15621

Howarth, R. W., Billen, G., Swaney, D., Townsend, A., Jaworski, N., Lajtha, K., Downing, J. A., Elmgren, R., Caraco, N., Jordan, T., Berendse, F., Freney, J., Kudeyarov, V., Murdoch, P., & Zhao-Liang, Z. (1996). Regional nitrogen budgets and riverine N & P fluxes for the drainages to the North Atlantic Ocean: Natural and human influences. Biogeochemistry, 35(1), 75–139. https://doi.org/10.1007/BF02179825

Hu, B., Shen, L., Lian, X., Zhu, Q., Liu, S., Huang, Q., He, Z., Geng, S., Cheng, D., Lou, L., Xu, X., Zheng, P., & He, Y. (2014). Evidence for nitrite-dependent anaerobic methane oxidation as a previously overlooked microbial methane sink in wetlands. Proceedings of the National Academy of Sciences, 111(12), 4495–4500. https://doi.org/10.1073/pnas.1318393111

Intergovernmental Panel on Climate Change (IPCC) (Ed.). (2023). Short-lived Climate Forcers. In Climate Change 2021 – The Physical Science Basis: Working Group I Contribution to the Sixth Assessment Report of the Intergovernmental Panel on Climate Change (pp. 817–922). Cambridge University Press. Cambridge Core. https://doi.org/10.1017/9781009157896.008

Iversen, N., & Jorgensen, B. B. (1985). Anaerobic methane oxidation rates at the sulfate-methane transition in marine sediments from Kattegat and Skagerrak (Denmark). Limnology and Oceanography, 30(5), 944–955. https://doi.org/10.4319/lo.1985.30.5.0944

Jackson, R. B., Saunois, M., Bousquet, P., Canadell, J. G., Poulter, B., Stavert, A. R., Bergamaschi, P., Niwa, Y., Segers, A., & Tsuruta, A. (2020). Increasing anthropogenic methane emissions arise equally from agricultural and fossil fuel sources. Environmental Research Letters, 15(7), 071002. https://doi.org/10.1088/1748-9326/ab9ed2

Jørgensen, B. B. (1982). Mineralization of organic matter in the sea bed—The role of sulphate reduction. Nature, 296(5858), 643–645. https://doi.org/10.1038/296643a0

Jørgensen, B. B. (2000). Bacteria and Marine Biogeochemistry. In H. D. Schulz & M. Zabel (Eds.), Marine Geochemistry (pp. 173–207). Springer Berlin Heidelberg. https://doi.org/10.1007/978-3-662-04242-7_5

Jørgensen, B. B., Beulig, F., Egger, M., Petro, C., Scholze, C., & Røy, H. (2019). Organoclastic sulfate reduction in the sulfate-methane transition of marine sediments. Geochimica et Cosmochimica Acta, 254, 231–245. https://doi.org/10.1016/j.gca.2019.03.016

Joye, S. B., Boetius, A., Orcutt, B. N., Montoya, J. P., Schulz, H. N., Erickson, M. J., & Lugo, S. K. (2004). The anaerobic oxidation of methane and sulfate reduction in sediments from Gulf of Mexico cold seeps. Chemical Geology, Geomicrobiology and Biogeochemistry of Gas Hydrates and Hydrocarbon Seeps, 205(3), 219–238. https://doi.org/10.1016/j.chemgeo.2003.12.019

Kallmeyer, J., Ferdelman, T. G., Weber, A., Fossing, H., & Jørgensen, B. B. (2004). A cold chromium distillation procedure for radiolabeled sulfide applied to sulfate reduction

measurements. Limnology and Oceanography: Methods, 2(6), 171–180. https://doi.org/10.4319/lom.2004.2.171

Kalyuzhnaya, M. G., Yang, S., Rozova, O. N., Smalley, N. E., Clubb, J., Lamb, A., Gowda, G. A. N., Raftery, D., Fu, Y., Bringel, F., Vuilleumier, S., Beck, D. a. C., Trotsenko, Y. A., Khmelenina, V. N., & Lidstrom, M. E. (2013). Highly efficient methane biocatalysis revealed in a methanotrophic bacterium. Nature Communications, 4(1), 2785. https://doi.org/10.1038/ncomms3785

Kana, T. M., Darkangelo, Christina., Hunt, M. Duane., Oldham, J. B., Bennett, G. E., & Cornwell, J. C. (1994). Membrane Inlet Mass Spectrometer for Rapid High-Precision Determination of N2, O2, and Ar in Environmental Water Samples. Analytical Chemistry, 66(23), 4166–4170. https://doi.org/10.1021/ac00095a009

Kintisch, E. (2013). Can Coastal Marshes Rise Above It All? Science, 341(6145), 480–481. https://doi.org/10.1126/science.341.6145.480

Knittel, K., & Boetius, A. (2009). Anaerobic Oxidation of Methane: Progress with an Unknown Process. Annual Review of Microbiology, 63(Volume 63, 2009), 311–334. https://doi.org/10.1146/annurev.micro.61.080706.093130

Knittel, K., Lösekann, T., Boetius, A., Kort, R., & Amann, R. (2005). Diversity and Distribution of Methanotrophic Archaea at Cold Seeps. Applied and Environmental Microbiology, 71(1), 467–479. https://doi.org/10.1128/AEM.71.1.467-479.2005

Knudsen, M. (1901). Hydrographical Tables According to the Measurings of Carl Forch [and Others] and with Assistance of Björn-Andersen [and Others]. G.E.C. Gad.

Koop-Jakobsen, K., & Giblin, A. E. (2009). Anammox in Tidal Marsh Sediments: The Role of Salinity, Nitrogen Loading, and Marsh Vegetation. Estuaries and Coasts, 32(2), 238–245. https://doi.org/10.1007/s12237-008-9131-y

Koop-Jakobsen, K., & Giblin, A. E. (2010). The effect of increased nitrate loading on nitrate reduction via denitrification and DNRA in salt marsh sediments. Limnology and Oceanography, 55(2), 789–802. https://doi.org/10.4319/lo.2010.55.2.0789

Krause, S. J. E., & Treude, T. (2021). Deciphering cryptic methane cycling: Coupling of methylotrophic methanogenesis and anaerobic oxidation of methane in hypersaline coastal wetland sediment. Geochimica et Cosmochimica Acta, 302, 160–174. https://doi.org/10.1016/j.gca.2021.03.021

Krause, S. J. E., Wipfler, R., Liu, J., Yousavich, D. J., Robinson, D., Hoyt, D. W., Orphan, V. J., & Treude, T. (2025). Spatial evidence of cryptic methane cycling and methylotrophic metabolisms along a land–ocean transect in salt marsh sediment. Geochimica et Cosmochimica Acta, 404, 53–71. https://doi.org/10.1016/j.gca.2025.07.019

Krekeler, D., & Cypionka, H. (1995). The preferred electron acceptor of Desulfovibrio desulfuricans CSN. FEMS Microbiology Ecology, 17(4), 271–277. https://doi.org/10.1111/j.1574-6941.1995.tb00151.x

Kristjansson, J. K., Schönheit, P., & Thauer, R. K. (1982). Different Ks values for hydrogen of methanogenic bacteria and sulfate reducing bacteria: An explanation for the apparent inhibition of methanogenesis by sulfate. Archives of Microbiology, 131(3), 278–282. https://doi.org/10.1007/BF00405893

La, W., Han, X., Liu, C.-Q., Ding, H., Liu, M., Sun, F., Li, S., & Lang, Y. (2022). Sulfate concentrations affect sulfate reduction pathways and methane consumption in coastal wetlands. Water Research, 217, 118441. https://doi.org/10.1016/j.watres.2022.118441

Lalk, E., Pohlman, J. W., & Lapham, L. L. (2025). Organic Matter Availability and the Production of Methane-Derived Dissolved Organic Carbon at Methane Seeps. Global Biogeochemical Cycles, 39(7), e2025GB008535. https://doi.org/10.1029/2025GB008535

Lapham, L. L., Lloyd, K. G., Fossing, H., Flury, S., Jensen, J. B., Alperin, M. J., Rehder, G., Holzhueter, W., Ferdelman, T., & Jørgensen, B. B. (2024). Methane leakage through the sulfate–methane transition zone of the Baltic seabed. Nature Geoscience, 17(12), 1277–1283. https://doi.org/10.1038/s41561-024-01594-z

Laso-Pérez, R., Krukenberg, V., Musat, F., & Wegener, G. (2018). Establishing anaerobic hydrocarbon-degrading enrichment cultures of microorganisms under strictly anoxic conditions. Nature Protocols, 13(6), 1310–1330. https://doi.org/10.1038/nprot.2018.030

Laufer, K., Michaud, A. B., Røy, H., & Jørgensen, B. B. (2020). Reactivity of Iron Minerals in the Seabed Toward Microbial Reduction – A Comparison of Different Extraction Techniques. Geomicrobiology Journal, 37(2), 170–189. https://doi.org/10.1080/01490451.2019.1679291

Laverman, A. M., Meile, C., Van Cappellen, P., & Wieringa, E. B. A. (2007). Vertical Distribution of Denitrification in an Estuarine Sediment: Integrating Sediment Flowthrough Reactor Experiments and Microprofiling via Reactive Transport Modeling. Applied and Environmental Microbiology, 73(1), 40–47. https://doi.org/10.1128/AEM.01442-06

Laverman, A. M., Pallud, C., Abell, J., & Cappellen, P. V. (2012). Comparative survey of potential nitrate and sulfate reduction rates in aquatic sediments. Geochimica et Cosmochimica Acta, 77, 474–488. https://doi.org/10.1016/j.gca.2011.10.033

Laverman, A. M., Van Cappellen, P., van Rotterdam-Los, D., Pallud, C., & Abell, J. (2006). Potential rates and pathways of microbial nitrate reduction in coastal sediments. FEMS Microbiology Ecology, 58(2), 179–192. https://doi.org/10.1111/j.1574-6941.2006.00155.x

Lee, J., Yang, Y., Kang, H., Noyce, G. L., & Megonigal, J. P. (2025). Climate-induced shifts in sulfate dynamics regulate anaerobic methane oxidation in a coastal wetland. Science Advances, 11(17), eads6093. https://doi.org/10.1126/sciadv.ads6093

Legg, S. (2021). IPCC, 2021: Climate Change 2021—The Physical Science basis. Interaction, 49(4), 44–45. (informit.315096509383738).

Legierse, A., Struik, Q., Smith, G., Echeveste Medrano, M. J., Weideveld, S., van Dijk, G., Smolders, A. J. P., Jetten, M., Veraart, A. J., Welte, C. U., & Glodowska, M. (2023). Nitrate-dependent anaerobic methane oxidation (N-DAMO) as a bioremediation strategy for waters affected by agricultural runoff. FEMS Microbiology Letters, 370, fnad041. https://doi.org/10.1093/femsle/fnad041

Leu, A. O., Cai, C., McIlroy, S. J., Southam, G., Orphan, V. J., Yuan, Z., Hu, S., & Tyson, G. W. (2020). Anaerobic methane oxidation coupled to manganese reduction by members of the Methanoperedenaceae. The ISME Journal, 14(4), 1030–1041. https://doi.org/10.1038/s41396-020-0590-x

Liu, J., Klonicki-Ference, E., Krause, S. J. E., & Treude, T. (2025). Iron Oxides Fuel Anaerobic Oxidation of Methane in the Presence of Sulfate in Hypersaline Coastal Wetland

Sediment. Environmental Science & Technology, 59(1), 513–522. https://doi.org/10.1021/acs.est.4c10639

Lorenzen, J., Larsen, L. H., Kjær, T., & Revsbech, N.-P. (1998). Biosensor Determination of the Microscale Distribution of Nitrate, Nitrate Assimilation, Nitrification, and Denitrification in a Diatom-Inhabited Freshwater Sediment. Applied and Environmental Microbiology, 64(9), 3264–3269. https://doi.org/10.1128/AEM.64.9.3264-3269.1998

Lovley, D. R., Coates, J. D., Blunt-Harris, E. L., Phillips, E. J. P., & Woodward, J. C. (1996). Humic substances as electron acceptors for microbial respiration. Nature, 382(6590), 445–448. https://doi.org/10.1038/382445a0

Lovley, D. R., Dwyer, D. F., & Klug, M. J. (1982). Kinetic Analysis of Competition Between Sulfate Reducers and Methanogens for Hydrogen in Sediments. Applied and Environmental Microbiology, 43(6), 1373–1379. https://doi.org/10.1128/aem.43.6.1373-1379.1982

Lovley, D. R., & Goodwin, S. (1988). Hydrogen concentrations as an indicator of the predominant terminal electron-accepting reactions in aquatic sediments. Geochimica et Cosmochimica Acta, 52(12), 2993–3003. https://doi.org/10.1016/0016-7037(88)90163-9

Lovley, D. R., & Klug, M. J. (1986). Model for the distribution of sulfate reduction and methanogenesis in freshwater sediments. Geochimica et Cosmochimica Acta, 50(1), 11–18. https://doi.org/10.1016/0016-7037(86)90043-8

Maltby, J., Steinle, L., Löscher, C. R., Bange, H. W., Fischer, M. A., Schmidt, M., & Treude, T. (2018). Microbial methanogenesis in the sulfate-reducing zone of sediments in the Eckernförde Bay, SW Baltic Sea. Biogeosciences, 15(1), 137–157. https://doi.org/10.5194/bg-15-137-2018

McGlynn, S. E., Chadwick, G. L., Kempes, C. P., & Orphan, V. J. (2015). Single cell activity reveals direct electron transfer in methanotrophic consortia. Nature, 526(7574), 531–535. https://doi.org/10.1038/nature15512

Meulepas, R. J. W., Jagersma, C. G., Gieteling, J., Buisman, C. J. N., Stams, A. J. M., & Lens, P. N. L. (2009). Enrichment of anaerobic methanotrophs in sulfate-reducing membrane bioreactors. Biotechnology and Bioengineering, 104(3), 458–470. https://doi.org/10.1002/bit.22412

Moffett, K. B., Robinson, D. A., & Gorelick, S. M. (2010). Relationship of Salt Marsh Vegetation Zonation to Spatial Patterns in Soil Moisture, Salinity, and Topography. Ecosystems, 13(8), 1287–1302. https://doi.org/10.1007/s10021-010-9385-7

Mostovaya, A., Wind-Hansen, M., Rousteau, P., Bristow, L. A., & Thamdrup, B. (2022). Sulfate- and iron-dependent anaerobic methane oxidation occurring side-by-side in freshwater lake sediment. Limnology and Oceanography, 67(1), 231–246. https://doi.org/10.1002/lno.11988

Murali, R., Yu, H., Speth, D. R., Wu, F., Metcalfe, K. S., Crémière, A., Laso-Pèrez, R., Malmstrom, R. R., Goudeau, D., Woyke, T., Hatzenpichler, R., Chadwick, G. L., Connon, S. A., & Orphan, V. J. (2023). Physiological potential and evolutionary trajectories of syntrophic sulfate-reducing bacterial partners of anaerobic methanotrophic archaea. PLOS Biology, 21(9), e3002292. https://doi.org/10.1371/journal.pbio.3002292

Nauhaus, K., Albrecht, M., Elvert, M., Boetius, A., & Widdel, F. (2007). In vitro cell growth of marine archaeal-bacterial consortia during anaerobic oxidation of methane with sulfate. Environmental Microbiology, 9(1), 187–196. https://doi.org/10.1111/j.1462-2920.2006.01127.x

Niemann, H., Steinle, L., Blees, J., Bussmann, I., Treude, T., Krause, S., Elvert, M., & Lehmann, M. F. (2015). Toxic effects of lab-grade butyl rubber stoppers on aerobic methane oxidation. Limnology and Oceanography: Methods, 13(1), 40–52. https://doi.org/10.1002/lom3.10005

Nisbet, E. G., Manning, M. R., Dlugokencky, E. J., Fisher, R. E., Lowry, D., Michel, S. E., Myhre, C. L., Platt, S. M., Allen, G., Bousquet, P., Brownlow, R., Cain, M., France, J. L., Hermansen, O., Hossaini, R., Jones, A. E., Levin, I., Manning, A. C., Myhre, G., … White, J. W. C. (2019). Very Strong Atmospheric Methane Growth in the 4 Years 2014–2017: Implications for the Paris Agreement. Global Biogeochemical Cycles, 33(3), 318–342. https://doi.org/10.1029/2018GB006009

Ocko, I. B., Sun, T., Shindell, D., Oppenheimer, M., Hristov, A. N., Pacala, S. W., Mauzerall, D. L., Xu, Y., & Hamburg, S. P. (2021). Acting rapidly to deploy readily available methane mitigation measures by sector can immediately slow global warming. Environmental Research Letters, 16(5), 054042. https://doi.org/10.1088/1748-9326/abf9c8

Oremland, R. S., & Polcin, S. (1982). Methanogenesis and Sulfate Reduction: Competitive and Noncompetitive Substrates in Estuarine Sediments. Applied and Environmental Microbiology, 44(6), 1270–1276. https://doi.org/10.1128/aem.44.6.1270-1276.1982

Oshkin, I. Y., Beck, D. A. C., Lamb, A. E., Tchesnokova, V., Benuska, G., McTaggart, T. L., Kalyuzhnaya, M. G., Dedysh, S. N., Lidstrom, M. E., & Chistoserdova, L. (2015). Methane-fed microbial microcosms show differential community dynamics and pinpoint taxa involved in communal response. The ISME Journal, 9(5), 1119–1129. https://doi.org/10.1038/ismej.2014.203

Ostrom, N. E., Gandhi, H., Trubl, G., & Murray, A. E. (2016). Chemodenitrification in the cryoecosystem of Lake Vida, Victoria Valley, Antarctica. Geobiology, 14(6), 575–587. https://doi.org/10.1111/gbi.12190

Page, H. M., Petty, R. L., & Meade, D. E. (1995). Influence of Watershed Runoff on Nutrient Dynamics in a Southern California Salt Marsh. Estuarine, Coastal and Shelf Science, 41(2), 163–180. https://doi.org/10.1006/ecss.1995.0059

Peng, X., Wilken, S. E., Lankiewicz, T. S., Gilmore, S. P., Brown, J. L., Henske, J. K., Swift, C. L., Salamov, A., Barry, K., Grigoriev, I. V., Theodorou, M. K., Valentine, D. L., & O'Malley, M. A. (2021). Genomic and functional analyses of fungal and bacterial consortia that enable lignocellulose breakdown in goat gut microbiomes. Nature Microbiology, 6(4), 499–511. https://doi.org/10.1038/s41564-020-00861-0

Petersen, S. G. G., Kristensen, E., & Quintana, C. O. (2023). Greenhouse Gas Emissions from Agricultural Land Before and After Permanent Flooding with Seawater or Freshwater. Estuaries and Coasts, 46(6), 1459–1474. https://doi.org/10.1007/s12237-023-01218-6

Pohlman, J. W., Bauer, J. E., Waite, W. F., Osburn, C. L., & Chapman, N. R. (2011). Methane hydrate-bearing seeps as a source of aged dissolved organic carbon to the oceans. Nature Geoscience, 4(1), 37–41. https://doi.org/10.1038/ngeo1016

Postma, D., & Jakobsen, R. (1996). Redox zonation: Equilibrium constraints on the Fe(III)/SO4-reduction interface. Geochimica et Cosmochimica Acta, 60(17), 3169–3175. https://doi.org/10.1016/0016-7037(96)00156-1

Poulton, S. W. (2021). The Iron Speciation Paleoredox Proxy. Elements in Geochemical Tracers in Earth System Science. https://doi.org/10.1017/9781108847148

Poulton, S. W., & Canfield, D. E. (2005). Development of a sequential extraction procedure for iron: Implications for iron partitioning in continentally derived particulates. Chemical Geology, 214(3), 209–221. https://doi.org/10.1016/j.chemgeo.2004.09.003

Prather, M. J., Holmes, C. D., & Hsu, J. (2012). Reactive greenhouse gas scenarios: Systematic exploration of uncertainties and the role of atmospheric chemistry. Geophysical Research Letters, 39(9). https://doi.org/10.1029/2012GL051440

Radajewski, S., McDonald, I. R., & Murrell, J. C. (2003). Stable-isotope probing of nucleic acids: A window to the function of uncultured microorganisms. Current Opinion in Biotechnology, 14(3), 296–302. https://doi.org/10.1016/S0958-1669(03)00064-8

Reeburgh, W. S. (2007). Oceanic Methane Biogeochemistry. Chemical Reviews, 107(2), 486–513. https://doi.org/10.1021/cr050362v

Riedinger, N., Formolo, M. J., Lyons, T. W., Henkel, S., Beck, A., & Kasten, S. (2014). An inorganic geochemical argument for coupled anaerobic oxidation of methane and iron reduction in marine sediments. Geobiology, 12(2), 172–181. https://doi.org/10.1111/gbi.12077

Rütting, T., Boeckx, P., Müller, C., & Klemedtsson, L. (2011). Assessment of the importance of dissimilatory nitrate reduction to ammonium for the terrestrial nitrogen cycle. Biogeosciences, 8(7), 1779–1791. https://doi.org/10.5194/bg-8-1779-2011

Sakoula, D., Smith, G. J., Frank, J., Mesman, R. J., Kop, L. F. M., Blom, P., Jetten, M. S. M., van Kessel, M. A. H. J., & Lücker, S. (2022). Universal activity-based labeling method for ammonia- and alkane-oxidizing bacteria. The ISME Journal, 16(4), 958–971. https://doi.org/10.1038/s41396-021-01144-0

Saunois, M., Martinez, A., Poulter, B., Zhang, Z., Raymond, P. A., Regnier, P., Canadell, J. G., Jackson, R. B., Patra, P. K., Bousquet, P., Ciais, P., Dlugokencky, E. J., Lan, X., Allen, G. H., Bastviken, D., Beerling, D. J., Belikov, D. A., Blake, D. R., Castaldi, S., … Zhuang, Q. (2025). Global Methane Budget 2000–2020. Earth System Science Data, 17(5), 1873–1958. https://doi.org/10.5194/essd-17-1873-2025

Scheller, S., Yu, H., Chadwick, G. L., McGlynn, S. E., & Orphan, V. J. (2016). Artificial electron acceptors decouple archaeal methane oxidation from sulfate reduction. Science, 351(6274), 703–707. https://doi.org/10.1126/science.aad7154

Schorn, S., Graf, J. S., Littmann, S., Hach, P. F., Lavik, G., Speth, D. R., Schubert, C. J., Kuypers, M. M. M., & Milucka, J. (2024). Persistent activity of aerobic methane-oxidizing bacteria in anoxic lake waters due to metabolic versatility. Nature Communications, 15(1), 5293. https://doi.org/10.1038/s41467-024-49602-5

Schubert, C. J., Vazquez, F., Lösekann-Behrens, T., Knittel, K., Tonolla, M., & Boetius, A. (2011). Evidence for anaerobic oxidation of methane in sediments of a freshwater system (Lago di Cadagno). FEMS Microbiology Ecology, 76(1), 26–38. https://doi.org/10.1111/j.1574-6941.2010.01036.x

Segarra, K. E. A., Comerford, C., Slaughter, J., & Joye, S. B. (2013). Impact of electron acceptor availability on the anaerobic oxidation of methane in coastal freshwater and brackish wetland sediments. Geochimica et Cosmochimica Acta, 115, 15–30. https://doi.org/10.1016/j.gca.2013.03.029

Segarra, K. E. A., Schubotz, F., Samarkin, V., Yoshinaga, M. Y., Hinrichs, K.-U., & Joye, S. B. (2015). High rates of anaerobic methane oxidation in freshwater wetlands reduce

potential atmospheric methane emissions. Nature Communications, 6(1), 7477. https://doi.org/10.1038/ncomms8477

Segers, R. (1998). Methane production and methane consumption: A review of processes underlying wetland methane fluxes. Biogeochemistry, 41(1), 23–51. https://doi.org/10.1023/A:1005929032764

Seitz, H.-J., & Cypionka, H. (1986). Chemolithotrophic growth ofDesulfovibrio desulfuricans with hydrogen coupled to ammonification of nitrate or nitrite. Archives of Microbiology, 146(1), 63–67. https://doi.org/10.1007/BF00690160

Shen, L., Hu, B., Liu, S., Chai, X., He, Z., Ren, H., Liu, Y., Geng, S., Wang, W., Tang, J., Wang, Y., Lou, L., Xu, X., & Zheng, P. (2016). Anaerobic methane oxidation coupled to nitrite reduction can be a potential methane sink in coastal environments. Applied Microbiology and Biotechnology, 100(16), 7171–7180. https://doi.org/10.1007/s00253-016-7627-0

Shen, L., Huang, Q., He, Z., Lian, X., Liu, S., He, Y., Lou, L., Xu, X., Zheng, P., & Hu, B. (2015). Vertical distribution of nitrite-dependent anaerobic methane-oxidising bacteria in natural freshwater wetland soils. Applied Microbiology and Biotechnology, 99(1), 349–357. https://doi.org/10.1007/s00253-014-6031-x

Shen, L., Wu, H., Liu, X., & Li, J. (2017). Cooccurrence and potential role of nitrite- and nitrate-dependent methanotrophs in freshwater marsh sediments. Water Research, 123, 162–172. https://doi.org/10.1016/j.watres.2017.06.075

Shi, Y., Ma, Q., Kuzyakov, Y., Sheng, L., Liu, H., & Wang, Z. (2022). Nitrite-dependent anaerobic oxidation decreases methane emissions from peatlands. Soil Biology and Biochemistry, 169, 108658. https://doi.org/10.1016/j.soilbio.2022.108658

Shi, Y., Wang, Z., He, C., Zhang, X., Sheng, L., & Ren, X. (2017). Using 13C isotopes to explore denitrification-dependent anaerobic methane oxidation in a paddy-peatland. Scientific Reports, 7(1), 40848. https://doi.org/10.1038/srep40848

Shindell, D., Kuylenstierna, J. C. I., Vignati, E., van Dingenen, R., Amann, M., Klimont, Z., Anenberg, S. C., Muller, N., Janssens-Maenhout, G., Raes, F., Schwartz, J., Faluvegi, G., Pozzoli, L., Kupiainen, K., Höglund-Isaksson, L., Emberson, L., Streets, D., Ramanathan, V., Hicks, K., … Fowler, D. (2012). Simultaneously Mitigating Near-Term Climate Change and Improving Human Health and Food Security. Science, 335(6065), 183–189. https://doi.org/10.1126/science.1210026

Sivan, O., Adler, M., Pearson, A., Gelman, F., Bar-Or, I., John, S. G., & Eckert, W. (2011). Geochemical evidence for iron-mediated anaerobic oxidation of methane. Limnology and Oceanography, 56(4), 1536–1544. https://doi.org/10.4319/lo.2011.56.4.1536

Slobodkin, A. I., Ratnikova, N. M., Slobodkina, G. B., Klyukina, A. A., Chernyh, N. A., & Merkel, A. Y. (2023). Composition and Metabolic Potential of Fe(III)-Reducing Enrichment Cultures of Methanotrophic ANME-2a Archaea and Associated Bacteria. Microorganisms, 11(3), 555. https://doi.org/10.3390/microorganisms11030555

Smith, V. H., Tilman, G. D., & Nekola, J. C. (1999). Eutrophication: Impacts of excess nutrient inputs on freshwater, marine, and terrestrial ecosystems. Environmental Pollution, 100(1), 179–196. https://doi.org/10.1016/S0269-7491(99)00091-3

Stookey, L. L. (1970). Ferrozine—A new spectrophotometric reagent for iron. Analytical Chemistry, 42(7), 779–781. https://doi.org/10.1021/ac60289a016

Strous, M., & Jetten, M. S. M. (2004). Anaerobic Oxidation of Methane and Ammonium. Annual Review of Microbiology, 58(Volume 58, 2004), 99–117. https://doi.org/10.1146/annurev.micro.58.030603.123605

Thamdrup, B., & Dalsgaard, T. (2002). Production of N2 through Anaerobic Ammonium Oxidation Coupled to Nitrate Reduction in Marine Sediments. Applied and Environmental Microbiology, 68(3), 1312–1318. https://doi.org/10.1128/AEM.68.3.1312-1318.2002

Thauer, R. K., Jungermann, K., & Decker, K. (1977). Energy conservation in chemotrophic anaerobic bacteria. Bacteriological Reviews, 41(1), 100–180. https://doi.org/10.1128/br.41.1.100-180.1977

Tiedje, J. M., Sexstone, A. J., Myrold, D. D., & Robinson, J. A. (1983). Denitrification: Ecological niches, competition and survival. Antonie van Leeuwenhoek, 48(6), 569–583. https://doi.org/10.1007/BF00399542

Timmers, P. H. A., Welte, C. U., Koehorst, J. J., Plugge, C. M., Jetten, M. S. M., & Stams, A. J. M. (2017). Reverse Methanogenesis and Respiration in Methanotrophic Archaea. Archaea, 2017, 1654237. https://doi.org/10.1155/2017/1654237

Timmers, P. H. A., Widjaja-Greefkes, H. C. A., Ramiro-Garcia, J., Plugge, C. M., & Stams, A. J. M. (2015). Growth and activity of ANME clades with different sulfate and sulfide concentrations in the presence of methane. Frontiers in Microbiology, 6. https://doi.org/10.3389/fmicb.2015.00988

United Nations Environment Programme and Climate & Clean Air Coalition. (2021). Global Methane Assessment: Benefits and Costs of Mitigating Methane Emissions. Nairobi: United Nations Environment Programme.

United States Environmental Protection Agency. (2004). Method 9060A: Total Organic Carbon (SW-846 Method No. 9060A). U.S. Environmental Protection Agency.

Valentine, D. L. (2002). Biogeochemistry and microbial ecology of methane oxidation in anoxic environments: A review. Antonie van Leeuwenhoek, 81(1), 271–282. https://doi.org/10.1023/A:1020587206351

Valenzuela, E. I., Avendaño, K. A., Balagurusamy, N., Arriaga, S., Nieto-Delgado, C., Thalasso, F., & Cervantes, F. J. (2019). Electron shuttling mediated by humic substances fuels anaerobic methane oxidation and carbon burial in wetland sediments. Science of The Total Environment, 650, 2674–2684. https://doi.org/10.1016/j.scitotenv.2018.09.388

Valenzuela, E. I., Prieto-Davó, A., López-Lozano, N. E., Hernández-Eligio, A., Vega-Alvarado, L., Juárez, K., García-González, A. S., López, M. G., & Cervantes, F. J. (2017). Anaerobic Methane Oxidation Driven by Microbial Reduction of Natural Organic Matter in a Tropical Wetland. Applied and Environmental Microbiology, 83(11), e00645-17. https://doi.org/10.1128/AEM.00645-17

van den Berg, E. M., Boleij, M., Kuenen, J. G., Kleerebezem, R., & van Loosdrecht, M. C. M. (2016). DNRA and Denitrification Coexist over a Broad Range of Acetate/N-NO3− Ratios, in a Chemostat Enrichment Culture. Frontiers in Microbiology, 7. https://doi.org/10.3389/fmicb.2016.01842

van Grinsven, S., Sinninghe Damsté, J. S., & Villanueva, L. (2020). Assessing the Effect of Humic Substances and Fe(III) as Potential Electron Acceptors for Anaerobic Methane Oxidation in a Marine Anoxic System. Microorganisms, 8(9), 1288. https://doi.org/10.3390/microorganisms8091288

Wallenius, A. J., Dalcin Martins, P., Slomp, C. P., & Jetten, M. S. M. (2021). Anthropogenic and Environmental Constraints on the Microbial Methane Cycle in Coastal Sediments. Frontiers in Microbiology, 12. https://doi.org/10.3389/fmicb.2021.631621

Wang, J., Cai, C., Li, Y., Hua, M., Wang, J., Yang, H., Zheng, P., & Hu, B. (2019). Denitrifying Anaerobic Methane Oxidation: A Previously Overlooked Methane Sink in Intertidal Zone. Environmental Science & Technology, 53(1), 203–212. https://doi.org/10.1021/acs.est.8b05742

Wang, J., Yao, X., Jia, Z., Zhu, L., Zheng, P., Kartal, B., & Hu, B. (2022). Nitrogen input promotes denitrifying methanotrophs' abundance and contribution to methane emission reduction in coastal wetland and paddy soil. Environmental Pollution, 302, 119090. https://doi.org/10.1016/j.envpol.2022.119090

Wegener, G., Krukenberg, V., Riedel, D., Tegetmeyer, H. E., & Boetius, A. (2015). Intercellular wiring enables electron transfer between methanotrophic archaea and bacteria. Nature, 526(7574), 587–590. https://doi.org/10.1038/nature15733

Wegener, G., Niemann, H., Elvert, M., Hinrichs, K.-U., & Boetius, A. (2008). Assimilation of methane and inorganic carbon by microbial communities mediating the anaerobic oxidation of methane. Environmental Microbiology, 10(9), 2287–2298. https://doi.org/10.1111/j.1462-2920.2008.01653.x

Whitmire, S. L., & Hamilton, S. K. (2005). Rapid Removal of Nitrate and Sulfate in Freshwater Wetland Sediments. Journal of Environmental Quality, 34(6), 2062–2071. https://doi.org/10.2134/jeq2004.0483

Winfrey, M. R., & Zeikus, J. G. (1977). Effect of sulfate on carbon and electron flow during microbial methanogenesis in freshwater sediments. Applied and Environmental Microbiology, 33(2), 275–281. https://doi.org/10.1128/aem.33.2.275-281.1977

Wissink, M., Glodowska, M., van der Kolk, M. R., Jetten, M. S. M., & Welte, C. U. (2024). Probing Denitrifying Anaerobic Methane Oxidation via Antimicrobial Intervention: Implications for Innovative Wastewater Management. Environmental Science & Technology, 58(14), 6250–6257. https://doi.org/10.1021/acs.est.3c07197

Wolfe, B. M., Lui, S. M., & Cowan, J. A. (1994). Desulfoviridin, a multimeric-dissimilatory sulfite reductase from Desulfovibrio vulgaris (Hildenborough) Purification, characterization, kinetics and EPR studies. European Journal of Biochemistry, 223(1), 79–89. https://doi.org/10.1111/j.1432-1033.1994.tb18968.x

Xiao, X., Luo, M., Zhang, C., Zhang, T., Yin, X., Wu, X., Zhao, J., Tao, J., Chen, Z., Liang, Q., & Dong, X. (2023). Metal-Driven Anaerobic Oxidation of Methane as an Important Methane Sink in Methanic Cold Seep Sediments. Microbiology Spectrum, 11(2), e05337-22. https://doi.org/10.1128/spectrum.05337-22

Xie, M., Zhang, X., Li, S., Maulani, N., Cai, F., Zheng, Y., Cai, C., Virdis, B., Yuan, Z., & Hu, S. (2024). Humic substances as electron acceptor for anaerobic oxidation of methane (AOM) and electron shuttle in Mn (IV)-dependent AOM. Science of The Total Environment, 912, 169576. https://doi.org/10.1016/j.scitotenv.2023.169576

Xue, H., Lang, Y., Ding, H., Han, X., Wang, T., Liu, Z., La, W., & Liu, C.-Q. (2024). Sulfate availability affect sulfate reduction pathways and methane consumption in freshwater wetland sediments. Applied Geochemistry, 176, 106215. https://doi.org/10.1016/j.apgeochem.2024.106215

Yang, S., Lv, Y., Liu, X., Wang, Y., Fan, Q., Yang, Z., Boon, N., Wang, F., Xiao, X., & Zhang, Y. (2020). Genomic and enzymatic evidence of acetogenesis by anaerobic methanotrophic archaea. Nature Communications, 11(1), 3941. https://doi.org/10.1038/s41467-020-17860-8

Yang, W., Shen, L., & Bai, Y. (2023). Role and regulation of anaerobic methane oxidation catalyzed by NC10 bacteria and ANME-2d archaea in various ecosystems. Environmental Research, 219, 115174. https://doi.org/10.1016/j.envres.2022.115174

Yin, G., Hou, L., Liu, M., Liu, Z., & Gardner, W. S. (2014). A Novel Membrane Inlet Mass Spectrometer Method to Measure 15NH4+ for Isotope-Enrichment Experiments in Aquatic Ecosystems. Environmental Science & Technology, 48(16), 9555–9562. https://doi.org/10.1021/es501261s

Yin, S. X., Chen, D., Chen, L. M., & Edis, R. (2002). Dissimilatory nitrate reduction to ammonium and responsible microorganisms in two Chinese and Australian paddy soils. Soil Biology and Biochemistry, 34(8), 1131–1137. https://doi.org/10.1016/S0038-0717(02)00049-4

Zhang, Y., Zhang, X., Wang, F., Xia, W., & Jia, Z. (2020). Exogenous nitrogen addition inhibits sulfate-mediated anaerobic oxidation of methane in estuarine coastal sediments. Ecological Engineering, 158, 106021. https://doi.org/10.1016/j.ecoleng.2020.106021

Zhang, Z., Zimmermann, N. E., Stenke, A., Li, X., Hodson, E. L., Zhu, G., Huang, C., & Poulter, B. (2017). Emerging role of wetland methane emissions in driving 21st century climate change. Proceedings of the National Academy of Sciences, 114(36), 9647–9652. https://doi.org/10.1073/pnas.1618765114

Zhao, Q., & Lu, Y. (2023). Anaerobic oxidation of methane in terrestrial wetlands: The rate, identity and metabolism. Science of The Total Environment, 902, 166049. https://doi.org/10.1016/j.scitotenv.2023.166049